








Article

New Hybrids of 4-Amino-2,3-polymethylene-quinoline and *p*-Tolylsulfonamide as Dual Inhibitors of Acetyl- and Butyrylcholinesterase and Potential Multifunctional Agents for Alzheimer's Disease Treatment

Galina F. Makhaeva ¹, Nadezhda V. Kovaleva ¹, Natalia P. Boltneva ¹, Sofya V. Lushchekina ^{1,2}, Tatiana Yu. Astakhova ², Elena V. Rudakova ¹, Alexey N. Proshin ¹, Igor V. Serkov ¹, Eugene V. Radchenko ^{1,3}, Vladimir A. Palyulin ^{1,3}, Sergey O. Bachurin ¹ and Rudy J. Richardson ^{4,5,6,*}

¹ Institute of Physiologically Active Compounds, Russian Academy of Sciences, 142432 Chernogolovka, Russia; gmakh@ipac.ac.ru (G.F.M.); kovalevanv@ipac.ac.ru (N.V.K.); boltneva@ipac.ac.ru (N.P.B.); sofya.lushchekina@gmail.com (S.V.L.); rudakova@ipac.ac.ru (E.V.R.); proshin@ipac.ac.ru (A.N.P.); serkoviv@mail.ru (I.V.S.); genie@qsar.chem.msu.ru (E.V.R.); vap@qsar.chem.msu.ru (V.A.P.); bachurin@ipac.ac.ru (S.O.B.)

² Emanuel Institute of Biochemical Physics, Russian Academy of Sciences, 119334 Moscow, Russia; astakhova1967.t@yandex.ru

³ Department of Chemistry, Lomonosov Moscow State University, 119991 Moscow, Russia

⁴ Department of Environmental Health Sciences, University of Michigan, Ann Arbor, MI 48109, USA

⁵ Department of Neurology, University of Michigan, Ann Arbor, MI 48109, USA

⁶ Center of Computational Medicine and Bioinformatics, University of Michigan, Ann Arbor, MI 48109, USA

* Correspondence: rjrich@umich.edu; Tel.: +1-734-936-0769

Academic Editor: Zrinka Kovarik

Received: 20 July 2020; Accepted: 24 August 2020; Published: 27 August 2020



Abstract: New hybrid compounds of 4-amino-2,3-polymethylene-quinoline containing different sizes of the aliphatic ring and linked to *p*-tolylsulfonamide with alkylene spacers of increasing length were synthesized as potential drugs for treatment of Alzheimer's disease (AD). All compounds were potent inhibitors of acetylcholinesterase (AChE) and butyrylcholinesterase (BChE) with selectivity toward BChE. The lead compound 4-methyl-N-(5-(1,2,3,4-tetrahydro-acridin-9-ylamino)-pentyl)-benzenesulfonamide (**7h**) exhibited an IC_{50} (AChE) = $0.131 \pm 0.01 \mu\text{M}$ (five times more potent than tacrine), IC_{50} (BChE) = $0.0680 \pm 0.0014 \mu\text{M}$, and $17.5 \pm 1.5\%$ propidium displacement at $20 \mu\text{M}$. The compounds possessed low activity against carboxylesterase, indicating a likely absence of unwanted drug-drug interactions in clinical use. Kinetics studies were consistent with mixed-type reversible inhibition of both cholinesterases. Molecular docking demonstrated dual binding sites of the conjugates in AChE and clarified the differences in the structure-activity relationships for AChE and BChE inhibition. The conjugates could bind to the AChE peripheral anionic site and displace propidium, indicating their potential to block AChE-induced β -amyloid aggregation, thereby exerting a disease-modifying effect. All compounds demonstrated low antioxidant activity. Computational ADMET profiles predicted that all compounds would have good intestinal absorption, medium blood-brain barrier permeability, and medium cardiac toxicity risk. Overall, the results indicate that the novel conjugates show promise for further development and optimization as multitarget anti-AD agents.

Keywords: 4-amino-2,3-polymethylene-quinoline; acetylcholinesterase (AChE); ADMET; Alzheimer's disease (AD); butyrylcholinesterase (BChE); molecular docking; *p*-tolylsulfonamide

1. Introduction

Alzheimer's disease (AD) is a common neurodegenerative disorder in the elderly that is manifested by progressive loss of memory and cognitive functions, which inevitably leads to disability and death [1]. The exact molecular mechanisms involved in AD initiation and progression are still unclear. However, it is obvious now that AD is a complex, multifactorial disorder and that advanced age is the main risk factor [2,3]. Several conditions are known to participate in the associated neurodegeneration. Accumulation of amyloid β peptide ($A\beta$) deposits, abnormal modification and accumulation of the tau protein accompanied by oxidative stress in the brain lead to synaptic dysfunction and neurodegeneration [4,5]. These processes most severely affect the cholinergic system and result in a progressive decrease in levels of the neurotransmitter acetylcholine (ACh) [6], which in turn produces the memory and cognitive deficits characteristic for patients with AD [7].

The anticholinesterase drugs donepezil (Aricept), galantamine (Reminyl), and rivastigmine (Exelon) are aimed at compensating the deficiency of ACh and are currently the main pharmacotherapeutic group used for the symptomatic treatment of AD [8–11]. These agents help to restore brain ACh levels by inhibiting cholinesterases, thereby increasing the duration of ACh action on postsynaptic receptors and enhancing cholinergic transmission. The brain contains two major forms of cholinesterases: acetylcholinesterase (AChE, EC 3.1.1.7) and butyrylcholinesterase (BChE, EC 3.1.1.8), which terminate cholinergic neurotransmission by the hydrolysis of ACh [12]. In a healthy brain, acetylcholine is predominantly (80%) hydrolyzed by AChE, whereas BChE plays a supplementary role serving as a co-regulator of AChE activity [13]. The cholinergic therapy of AD was originally directed primarily toward the inhibition of AChE [11,14]. However, with progression of AD, the activity of AChE decreases while the activity of BChE gradually increases [13,15,16]. This enlarges the significance of BChE as an additional therapeutic target for reducing the cholinergic deficiency inherent in AD [17–20]. Selective inhibitors of BChE can increase the brain level of acetylcholine and enhance cognitive functions in rodents without the usual side effects typical of AChE inhibitors [17,18,21]. It is believed that compounds inhibiting both cholinesterases increase the efficiency of treatment [19,20,22]. However, although these medications can temporarily reduce the development of AD symptoms, they cannot stop the progression of neurodegeneration [8,14].

The formation of β -amyloid ($A\beta$) deposits is typical of the early pathogenesis in AD. Many lines of evidence suggest that both AChE and BChE, which are localized within $A\beta$ plaques in the AD brain, are related to amyloid plaque formation and thus contribute to the neuropathology of the disease [23–25]. AChE has proaggregant properties toward β -amyloid via involvement of the AChE peripheral anionic site (PAS) located at the rim of the gorge, which interacts with soluble β -amyloid peptides, thus promoting their aggregation [24,26–29]. It has been found that PAS ligands, such as propidium, block AChE-induced $A\beta$ aggregation by physically hampering $A\beta$ binding to the enzyme surface [26,27,30]. Moreover, dual-binding molecules, which interact with both the catalytic active site (CAS) and the PAS of AChE, can inhibit AChE activity and block its amyloidogenic properties. Such compounds not only can cause alleviation of the cognitive impairment of AD individuals via increasing the levels of acetylcholine but also can play a role as disease-modifying agents that can delay the formation of $A\beta$ plaques [28,31–34]. BChE is also involved in the formation and/or maturation of $A\beta$ plaques and thereby contributes to the pathogenesis of AD [15,35]. Therefore, inhibitors of both cholinesterases are of interest from the point of view of anti-amyloid strategy.

Currently, the multifactorial nature of AD has changed the approach to searching for effective drugs from the concept of single-target molecules to the design of multi-target agents that can simultaneously modulate multiple biological targets involved in disease pathogenesis [3,36–39]. Cholinesterases are still the most promising targets for ameliorating cognitive dysfunctions in AD. Accordingly, in the design of multi-target drugs, a cholinesterase inhibitor is selected as one of the pharmacophores. A second pharmacophore is then attached via a spacer to the cholinesterase inhibitor [40–44]. Such hybrid molecules expand the range of pharmacological activities of a parent anticholinesterase compound by adding antiaggregant, antioxidant, and other desirable properties [45–50].

Tacrine is the first drug approved for AD treatment. It has a high affinity for the AChE CAS and is widely employed as a pharmacophore to create multifunctional cholinesterase inhibitors possessing additional neuroprotective and disease-modifying properties [46,51–57].

In the present work, we used 4-amino-2,3-polymethylene-quinoline with different sizes of the aliphatic ring as the main anticholinesterase pharmacophore (Figure 1A); the homologue with $n = 2$ is tacrine.

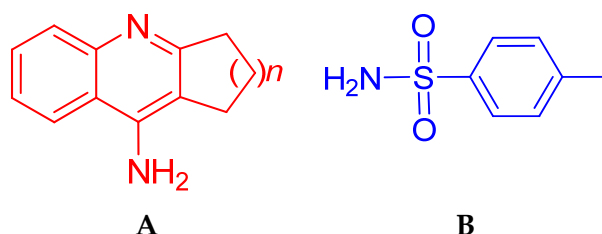


Figure 1. Structures of pharmacophores: (A) 4-amino-2,3-polymethylene-quinolines; (B) *p*-tolylsulfonamide.

The aromatic *p*-tolylsulfonamide moiety (Figure 1B) was used as our second pharmacophore. Sulfonamides are widely utilized in various pharmaceutical applications due to their therapeutic versatility that encompasses antibacterial, antiviral, antimalarial, antifungal, anticancer, antidepressant, and other properties [58,59]. They are also among the most effective and highly investigated derivatives in the field of carbonic anhydrases inhibition and related clinical applications [60–62]. Recently, publications have appeared on the presence of inhibitory activity against AChE and BChE in various sulfonamide derivatives [63–67]. Sulfonamide-containing selective and reversible human BChE inhibitors with nanomolar potency were developed that improved learning and memory functions in mouse models [21]. Moreover, antioxidant activity has been shown for certain sulfonamide derivatives [65,66,68,69]. Several sulfonamide-containing compounds exhibited promising A β self-assembly and cholinesterase inhibition, and in parallel showed good free radical scavenging properties [63].

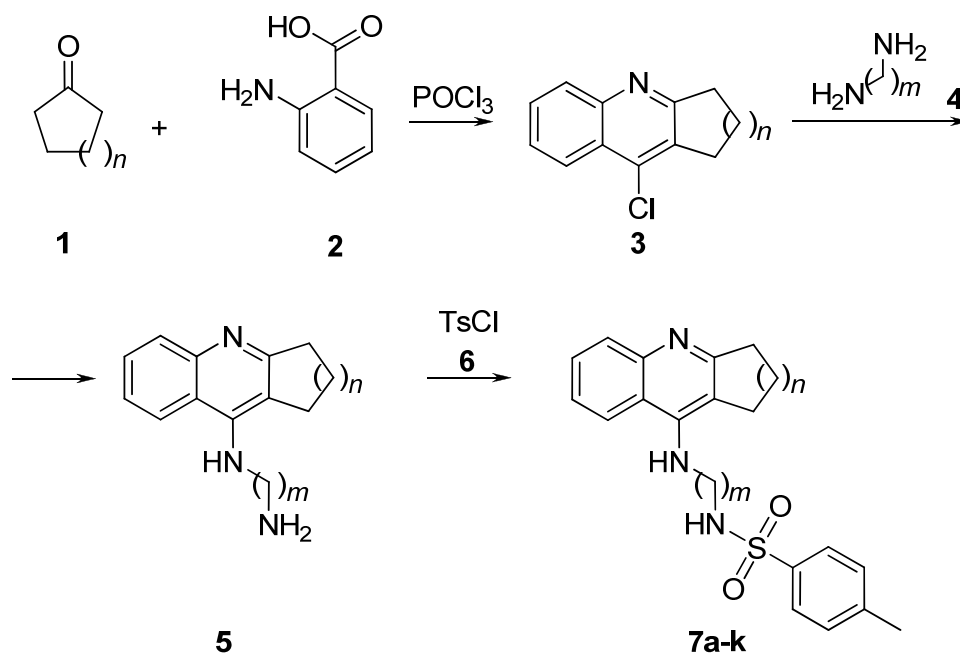
The incorporation of a sulfonamide fragment into hybrid structures for anti-AD drugs has likewise been demonstrated. For example, a series of tacrine derivatives containing a sulfonamide group was synthesized; the compounds exhibited potent inhibitory activity on both cholinesterases and were shown to have antioxidant properties [69]. In addition, quinoline-sulfonamide hybrids have been developed as potential multifunctional therapeutic agents for AD with high anti-AChE and anti-BChE activity; the lead compound in this series was shown to improve hippocampal-dependent working memory in a rat model [70].

Herein, we have synthesized new hybrid compounds of 4-amino-2,3-polymethylene-quinoline containing different sizes of the aliphatic ring and linked to *p*-tolylsulfonamide using alkylene spacers of increasing length. We investigated the action of the synthesized compounds on enzyme targets of the cholinergic nervous system using as surrogates human erythrocyte acetylcholinesterase (EC 3.1.1.7, AChE) and equine serum butyrylcholinesterase (EC 3.1.1.8, BChE), along with a structurally related enzyme, porcine liver carboxylesterase (EC 3.1.1.1, CES). We also studied the ability of our novel conjugates to bind to the PAS of AChE from *Electrophorus electricus* (EeAChE) and competitively displace propidium iodide from this site as a measure of their potential ability to block AChE-induced aggregation of β -amyloid. Enzyme kinetics studies were used to ascertain the mechanism of inhibition, and molecular docking was employed to provide insights into the binding modes of conjugates in the AChE and BChE active sites. We also measured the radical-scavenging activity of the conjugates in the ABTS assay. Finally, to assess the potential pharmacokinetic properties of the new compounds, we computationally estimated their profiles for absorption, distribution, metabolism, excretion, and toxicity (ADMET). Some preliminary results have been published earlier [71].

2. Results and Discussion

2.1. Chemistry

We have developed a method for the synthesis of hybrid multi-target compounds **7a–k** based on 4-amino-2,3-polymethylene-quinolines as the first pharmacophore and *p*-tolylsulfonamide as the second pharmacophore. Previously, we synthesized such compounds **7b,f,i,k** in which the quinoline and sulfonamide pharmacophores were combined into one molecule with a diaminopropane linker, in the form of hydrochlorides [71]. Here, we devised a procedure for the synthesis of target conjugates in the form of free bases. As shown in Figure 2, these compounds were obtained by the reaction of aminoquinolines **5** with tosyl chloride **6** in the presence of triethylamine. The aminoquinolines **5** needed for this were synthesized by the following method. First, by boiling anthranilic acid (**2**) with ketones **1** (cyclopentanone, cyclohexanone, cycloheptanone or cyclooctanone) in phosphorus oxychloride, chlorine derivatives **3** were obtained. Then, derivatives **3** were condensed with diamines **4** according to a published procedure [72] to afford the necessary aminoquinolines **5**.



$$n = 1-4, m = 2-6;$$

7: $n = 1, m = 2$ (**a**), $n = 1, m = 3$ (**b**), $n = 1, m = 4$ (**c**), $n = 1, m = 5$ (**d**), $n = 1, m = 6$ (**e**);
 $n = 2, m = 3$ (**f**), $n = 2, m = 4$ (**g**), $n = 2, m = 5$ (**h**);
 $n = 3, m = 3$ (**i**), $n = 3, m = 4$ (**j**); $n = 4, m = 3$ (**k**)

Figure 2. Synthesis of conjugates of 4-amino-2,3-polymethylene-quinolines and *p*-tolylsulfonamide **7**.

Thus, conjugates **7** with different sizes of the aliphatic ring of 4-amino-2,3-polymethylene-quinolines and various lengths of the alkyl chain linking the two pharmacophores have been synthesized. The size of the aliphatic ring and the length of the alkyl spacer for each compound **7** are shown in Table 1.

Table 1. Esterase profile of conjugates **7** and their ability to displace propidium.

Compound			Inhibitory Activity Against AChE, BChE and CES and Inhibitor Selectivity				Displacement of Propidium from the EeAChE PAS, (%) ¹
N	n	m	Human Erythrocyte AChE, IC ₅₀ (μM)	Equine Serum BChE, IC ₅₀ (μM)	Porcine Liver CES, (%) ¹	Selectivity, S = IC ₅₀ AChE/IC ₅₀ BChE	
7a	1	2	9.03 ± 0.64	0.924 ± 0.031	11.9 ± 1.5	9.8	9.2 ± 1.0
7b	1	3	7.76 ± 0.61	0.327 ± 0.004	8.1 ± 0.6	23.7	12.3 ± 1.1
7c	1	4	2.08 ± 0.08	0.578 ± 0.025	9.0 ± 0.1	3.6	14.9 ± 1.2
7d	1	5	1.97 ± 0.05	0.459 ± 0.044	29.6 ± 1.2	4.3	15.1 ± 1.4
7e	1	6	4.00 ± 0.09	0.209 ± 0.008	18.6 ± 0.2	1.9	15.9 ± 1.3
7f	2	3	1.88 ± 0.03	0.110 ± 0.005	2.0 ± 0.8	17.1	9.8 ± 0.8
7g	2	4	0.668 ± 0.17	0.0617 ± 0.0003	17.1 ± 1.4	10.8	14.8 ± 1.3
7h	2	5	0.131 ± 0.01	0.0680 ± 0.0014	6.7 ± 0.8	1.9	17.5 ± 1.5
7i	3	3	2.76 ± 0.04	0.0431 ± 0.0011	1.9 ± 0.9	64.0	13.9 ± 1.3
7j	3	4	1.16 ± 0.03	0.0788 ± 0.006	10.3 ± 0.8	14.7	16.1 ± 1.4
7k	4	3	11.1 ± 0.2	0.461 ± 0.007	5.2 ± 1.5	24.1	15.9 ± 1.7
Tacrine			0.601 ± 0.047	0.0295 ± 0.0020	n.a.	20.4	4.4 ± 0.6
Donepezil			0.040 ± 0.004	19.2 ± 3.0	n.a.	0.002	10.1 ± 0.6
BNPP			n.a.	n.a.	1.80 ± 0.11	n.d.	n.d.

¹ compound concentration 20 μM. n.a.—not active. n.d.—not determined. Data are presented as means ± SEM, n = 3.

2.2. Inhibition Studies of AChE, BChE and CES. Structure-Activity Relationships

For all conjugates **7**, we determined their esterase profile, i.e., the relative ability to inhibit several related serine esterases – AChE, BChE, and CES. This approach makes it possible to estimate both the primary pharmacological effects of the tested compounds (the inhibition of AChE and BChE) and their possible unwanted side effects (the inhibition of CES that hydrolyzes numerous ester-containing drugs) [73–77]. AChE from human erythrocytes was used along with two enzymes of non-human origin: equine serum BChE and porcine liver CES. These sources of BChE and CES were used because of their relatively low cost, high sequence identity to human enzymes [73,74,76], and the exploratory character of this work.

The inhibitory activities of our conjugates against the esterases were characterized as IC₅₀ values, i.e., the inhibitor concentrations required to decrease a given enzyme activity by 50%. Tacrine, an effective AChE and BChE inhibitor, and bis-4-nitrophenyl phosphate (BNPP), a selective CES inhibitor, were used as positive controls. The results are shown in Table 1.

As can be seen from Table 1, conjugates **7** generally inhibited both cholinesterases effectively, exhibiting, like tacrine, a higher activity toward BChE. The activities of compounds **7b**, **7f**, **7i**, **7k** obtained here coincided with the previously determined results [71]. Conjugates **7** practically did not inhibit CES, which suggests that potential unwanted drug-drug interactions would be lacking if these compounds were used clinically for AD treatment.

The degree and selectivity of enzyme inhibition was found to be determined by the structure of the synthesized conjugates; namely, the aliphatic ring size of the 4-amino-2,3-polymethylene-quinoline fragment (i.e., the tacrine moiety) and the length of the spacer linking the pharmacophores. The effect of the aliphatic ring size was demonstrated by compounds **7b**, **7f**, **7i**, **7k** with a spacer length $m = 3$ (Table 1). The most active compound toward AChE was conjugate **7f** with an unmodified six-membered tacrine ring (C-6, $n = 2$), whose inhibitory activity was only three times lower than that of tacrine. The conjugate **7i** with a seven-membered tacrine ring (C-7, $n = 3$) exhibited maximum activity toward BChE: it inhibited the enzyme in the nanomolar range with an IC₅₀ = 0.044 μM, close to that of tacrine. An increase in the size of the aliphatic ring to 8 (C-8, **7k**) reduced the anti-AChE activity ten-fold and decreased anti-BChE activity six-fold. Thus, the six-membered aliphatic ring of tacrine

was optimal for the anti-AChE activity of conjugates **7**, whereas a 7-membered ring was best for their anti-BChE potency.

An increase in the spacer length (m) for conjugates with the same ring size in series **7a–7e** (C-5, $n = 1$), **7f–7h** (C-6, $n = 2$), and **7i–7j** (C-7, $n = 3$) led to an increase in the inhibitory activity of compounds toward AChE. The most active among compounds with a five-membered ring were compounds **7c** and **7d** containing four and five methylene groups, respectively. In a series of compounds with a six-membered tacrine aliphatic ring **7f–7h** (C-6, $n = 2$), the inhibitory activity toward AChE increased more than 14 times with an increase in the length of the spacer from three to five CH₂ groups. Compound **7h** exhibited the maximum anti-AChE activity, being five times more potent than tacrine.

The results are consistent with the known data that, in contrast to extremely powerful bis-tacrine inhibitors [78], tacrine-based hybrid compounds linking tacrine with an uncharged aromatic group had anti-AChE activities comparable to that of tacrine [79,80].

In the case of anti-BChE activity, it was not possible to reveal a clear pattern of the dependence of enzyme inhibition on the spacer length of the conjugate. The maximum anti-BChE activity, close to that of tacrine, was found for compounds **7g** and **7h** with a six-membered tacrine ring and a spacer length of four and five CH₂ groups, respectively, as well as for compounds **7i** and **7j** with a seven-membered tacrine aliphatic ring and a spacer length of three and four CH₂ groups, respectively.

Regarding inhibitory selectivity, all conjugates **7** were more selective toward BChE, with selectivity factors ranging from 1.9 to 64. Conjugates with a rather short propylene spacer (**7b**, **7f**, **7i** and **7k**) exhibited maximum selectivity for BChE ($S = 17.1–64.0$). The most selective was conjugate **7i** with a 7-membered aliphatic ring.

2.3. Kinetic Studies of AChE and BChE Inhibition

The mechanism of inhibitory action of conjugates **7** towards AChE and BChE was studied using compound **7g** as an example. The graphical analysis of the kinetic data on AChE (Figure 3A) and BChE (Figure 3B) inhibition by **7g** in the Lineweaver–Burk double-reciprocal plot demonstrates the changes in both K_m and V_{max} that attests to a mixed type of inhibition. The inhibition constants were $K_i = 0.390 \pm 0.008 \mu\text{M}$ (competitive component) and $\alpha K_i = 1.09 \pm 0.02 \mu\text{M}$ (noncompetitive component) for AChE and $K_i = 0.0235 \pm 0.0002 \mu\text{M}$ (competitive component) and $\alpha K_i = 0.117 \pm 0.002 \mu\text{M}$ (noncompetitive component) for BChE.

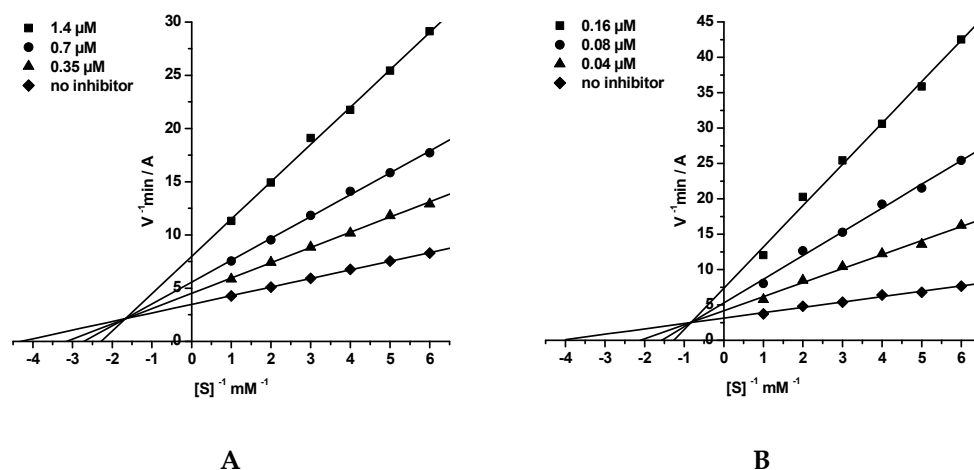


Figure 3. Steady state inhibition of (A) AChE and (B) BChE by compound **7g**. Lineweaver-Burk double-reciprocal plots of initial velocity and substrate concentrations in the presence of inhibitor (three concentrations) and without inhibitor are presented. The changes in both K_m and V_{max} attest to a mixed type of inhibition.

2.4. Molecular Docking Studies

The differential interaction of bulky inhibitors with AChE and BChE is highly dependent on the difference in structure of the active site gorge that leads from the protein surface to the active site [49,50,81–84]. AChE has a narrow gorge divided by the so-called bottleneck into the PAS and CAS [85,86]. The AChE gorge is lined with aromatic residues that favor binding of positively charged substrates/inhibitors, and the dynamically changing radius of the bottleneck determines the kinetics of binding; in particular, slow-binding inhibition [87,88]. BChE has a wider gorge than AChE without a pronounced narrowing to separate the PAS and CAS, and most of the BChE gorge residues that are aromatic in AChE are replaced in BChE with aliphatic ones [86]. This makes the BChE gorge more permissive to uncharged or even negatively charged substrates and inhibitors [89], and less prone to slow-binding inhibition than is the case with AChE [90,91].

Molecular docking of conjugates **7** into AChE demonstrated that they are dual binding-site inhibitors. This confirms our previous finding [49,71]. The tacrine fragment binds in the CAS and the *p*-tolylsulfonamide moiety binds to the PAS. Comparison of docking results of the compounds to different X-ray structures of human AChE showed that the best binding poses were obtained with the X-ray structure of AChE co-crystallized with donepezil (PDB: 4EY7). This structure has conformational changes of CAS and PAS amino acids necessary to accommodate bulky inhibitors [92].

Molecular docking of compounds **7b**, **7f**, **7i**, **7k** with the spacer $m = 3$ explains the observed effect of the aliphatic ring size on the inhibitory activity toward AChE. The position of the 4-amino-2,3-polymethylene-quinoline (tacrine) ring inside the AChE active site is similar for compounds **7b**, **7f**, **7i**, but not for compound **7k** with the largest C-8 aliphatic ring (Figure 4A). The increased size of the aliphatic ring does not allow it to fit in the same region below the bottleneck; the displaced C-8 tacrine ring leads to the loss of a hydrogen bond between the protonated amino group of the tacrine fragment and the Tyr124 side chain. This results in the experimentally observed reduced binding affinity.

In the case of binding to BChE, the influence of the aliphatic ring size is not as pronounced as with AChE; all tacrine fragments are located inside the BChE gorge in a uniform way (Figure 4B), with the sulfonamide group binding to the active site and forming hydrogen bonds with catalytic residues and the oxyanion hole. The protonated amino group in the tacrine fragment forms ionic interactions with Asp70 in the PAS. However, for compound **7k** (C-8), the large aliphatic ring size impairs ionic interactions of the positively charged external amino group of the tacrine fragment with the Asp70 anionic side chain. Otherwise, compound **7i** with a 7-membered ring did not have more specific interactions than compounds **7b** and **7f**, but it appeared to fit better than the others in the active site gorge cavity.

As was observed earlier for other dual binding site AChE inhibitors with lengthy spacers [49,50,81–84], they are located inside the AChE gorge in an elongated conformation whereas they are bent inside the wider BChE gorge. Consequently, an increase in the spacer length for conjugates with the same ring size leads to better occupation of the AChE PAS by the *p*-tolylsulfonamide fragment. Figure 4C shows binding poses of compounds **7a–7e** (C-5) as an example, while for compounds **7f–7h** (C-6) the same trend was observed. Although for the compounds with a shorter linker (**7a**, **7b**) hydrogen bonding between the sulfo-group and the Tyr124 side chain is possible while no specific interactions of the conjugate molecules in the PAS were observed, more favorable occupancy of the PAS by compounds with a longer linker leads to better propidium displacement and increased inhibitory activity due to hydrophobic interactions. In contrast, the position of the compounds inside the BChE gorge was almost unaffected by spacer length (Figure 4D), in accordance with the weak influence of the spacer length on experimentally measured inhibitory activities.

Thus, the molecular docking results show that the differences in the structure of the active sites of AChE and BChE give rise to different structure-inhibitory activity relationships for inhibition of these enzymes by these hybrid inhibitors.

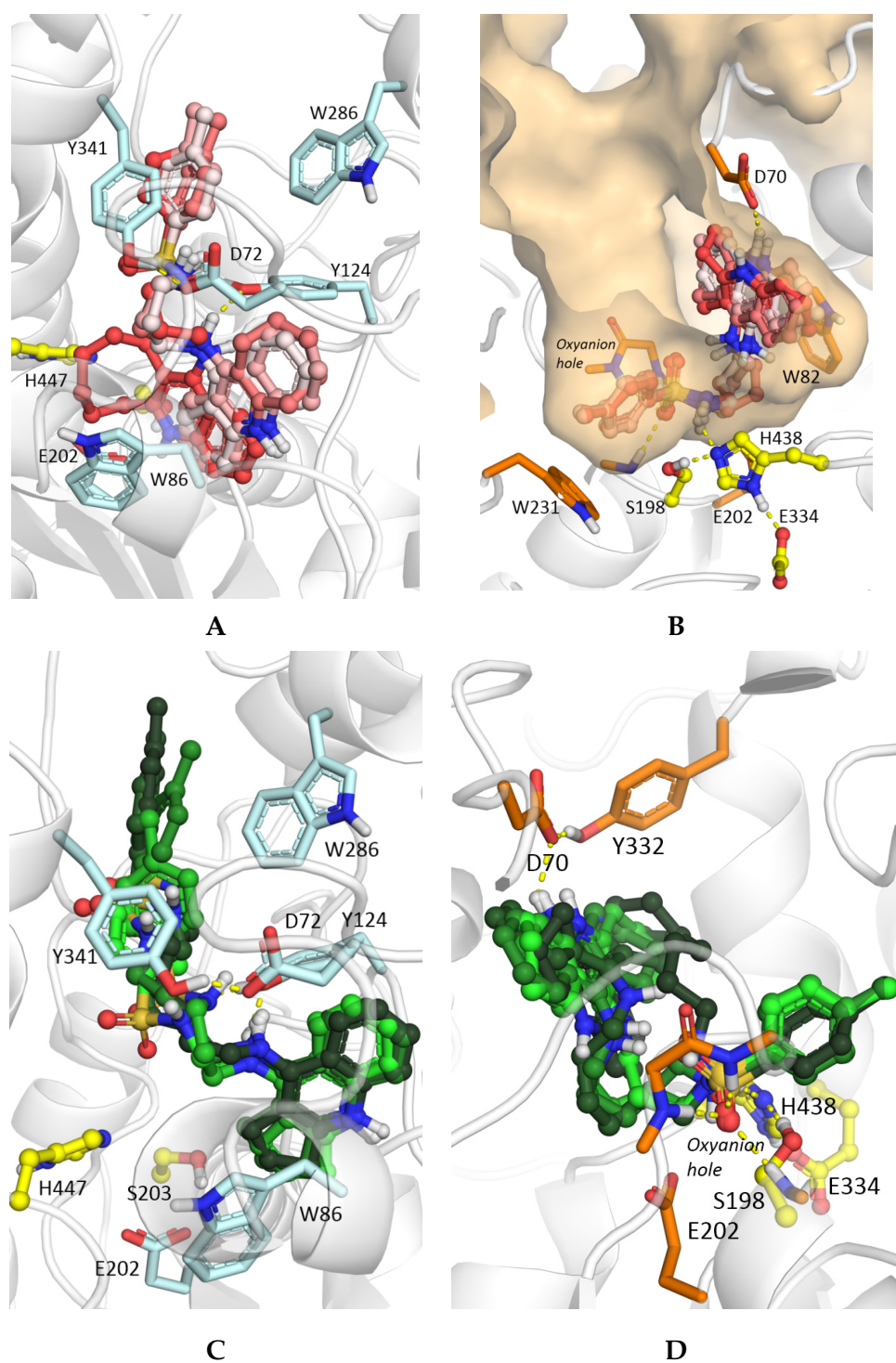


Figure 4. Results of molecular docking of hybrids of 4-amino-2,3-polymethylene-quinoline and *p*-tolylsulfonamide **7** into AChE (carbon atoms are shown in pale blue) and BChE (carbon atoms are shown in orange). The surface shows the gorge leading from the protein surface to the active site with a hollow space accommodating the aliphatic ring of the tacrine fragment of compounds **7**. Compounds **7b**, **7f**, **7i**, **7k** with $m = 3$ spacers and increasing aliphatic ring size (carbon atoms are shown with different shades of red from pale for **7b** (C-5) to bright for **7k** (C-8) inside (A) AChE and (B) BChE. Compounds **7a–7e** with C-5 aliphatic rings and increasing spacer length (carbon atoms are shown with different shades of green from pale for **7a** ($m = 2$) to dark for **7e** ($m = 6$) inside (C) AChE and (D) BChE.

2.5. Displacement of Propidium Iodide from the PAS of EeAChE

Propidium is a selective ligand for the PAS of AChE responsible for the A β binding [24,29,30,93], which showed a significant decrease in AChE-induced A β aggregation (82% at 100 μ M) [26]. This observation has served as the basis for the fluorescent evaluation of competitive propidium displacement from the PAS of AChE as a screening method to assess the potential ability of compounds to bind PAS and thus block the pro-aggregation activity of AChE [28]. Propidium iodide exhibits a fluorescence increase upon binding to AChE. A decrease in propidium fluorescence in the presence of test compounds indicates that they are able to displace propidium and bind to the PAS of AChE, suggesting that they would thereby block the AChE-mediated aggregation of β -amyloid [24,27,29,33]. Here, donepezil was used as a reference compound. Donepezil is a mixed-type AChE inhibitor, for which the ability to block AChE-PAS-induced A β aggregation has been demonstrated [26]. The results are presented in Table 1.

It can be seen in Table 1 that the sulfonamide-containing conjugates **7** at a concentration of 20 μ M reduced the fluorescence intensity by 9–17% and more effectively displaced propidium from the PAS of AChE compared to the reference compound donepezil. For compounds **7f**, **i**, there were no differences with the results obtained earlier [71]. For all 4-amino-2,3-polymethylene-quinoline-sulfonamide heterodimers with five, six, or seven-membered aliphatic rings, the degree of propidium displacement increased with elongation of the spacer length, which agrees with the results of molecular docking.

Taken together, the results from propidium displacement, kinetics, and molecular docking indicate that the conjugates **7** are dual-site AChE inhibitors occupying both CAS and PAS pockets. Thanks to binding to the PAS of AChE, they can potentially block AChE-induced aggregation of β -amyloid, thus having an additional positive disease modification effect.

2.6. Antioxidant Activity

The presence of antioxidant activity in a number of sulfonamide derivatives [66,68,69] prompted us to assess the antioxidant properties of the new hybrid compounds. A study of the antioxidant activity of conjugates **7** in the ABTS test showed that the binding of the ABTS radical by these conjugates is rather weak in comparison with the standard antioxidant, Trolox. TEAC values = 0.06–0.13 (TEAC values are expressed as Trolox equivalents calculated from $(A_0 - A_{\text{test}})/(A_0 - A_{\text{Trolox}})$ at 20 μ M concentrations, where A_0 is the absorbance of a control lacking any radical scavenger, A_{test} and A_{Trolox} are the absorbances of the remaining ABTS $^{\bullet+}$ in the presence of the test compound or Trolox, respectively).

2.7. Predicted ADMET Profiles and PAINS Analysis

The results of the computational estimation of a number of ADMET and physicochemical properties for the compounds **7a–k** are shown in Table 2. As can be seen, all of the compounds had high predicted values for intestinal absorption, enabling their oral administration. Thanks to moderate predicted blood-brain barrier permeability (brain concentration is about 10–25% of the plasma concentration), sufficient CNS activity can be expected. Both parameters of the cardiac toxicity risk (pK_i and pIC_{50}) for all analyzed compounds (4.7–6.5 log units) are in the lower or medium part of their possible range (3–9 log units). Although these values are acceptable, additional studies and structure optimization are desirable for a few compounds in order to ensure maximal safety. The predicted lipophilicities and aqueous solubilities of the compounds are also good for potential drug compounds. The integral quantitative estimates of drug-likeness (QED) are above 0.3 for all the compounds and above 0.5 for most of them. The Pan Assay INterference compoundS (PAINS) filter check for the compounds listed in Table 2 did not identify any structural alerts. Thus, the predicted ADMET, physicochemical, and PAINS properties of the compounds **7a–k** are quite acceptable for potential lead compounds at the early drug development stages.

Table 2. Predicted ADMET and physicochemical profiles of conjugates 7.

Compound			LogBB	HIA%	hERG, pK_i	hERG, pIC_{50}	LogPow	pS	QED
N	n	m							
7a	1	2	−0.94	97	4.67	5.54	2.89	3.60	0.64
7b	1	3	−0.86	100	4.88	5.76	3.21	3.73	0.60
7c	1	4	−0.78	100	4.96	6.14	3.62	4.02	0.55
7d	1	5	−0.70	100	5.25	6.18	4.04	4.34	0.49
7e	1	6	−0.63	100	5.03	6.35	4.47	4.68	0.44
7f	2	3	−0.78	100	4.92	5.64	3.71	4.09	0.57
7g	2	4	−0.70	100	5.25	6.02	4.09	4.38	0.52
7h	2	5	−0.63	100	5.30	6.37	4.49	4.70	0.46
7i	3	3	−0.70	100	4.93	5.75	4.11	4.40	0.43
7j	3	4	−0.63	100	5.01	6.46	4.48	4.69	0.38
7k	4	3	−0.63	100	5.04	5.91	4.55	4.75	0.51

Note: LogBB—blood-brain barrier permeability, HIA—human intestinal absorption [%], hERG pK_i —hERG potassium channel affinity [−log(M)], hERG pIC_{50} —hERG potassium channel inhibitory activity [−log(M)], LogPow—octanol-water partition coefficient, pS—aqueous solubility [−log(M)], QED—quantitative estimate of drug-likeness.

3. Materials and Methods

3.1. Chemistry

All solvents, chemicals, and reagents were obtained commercially and used without purification. $^1\text{H-NMR}$ (200 MHz) spectra were recorded on a DPX-200 NMR spectrometer (Bruker, Karlsruhe, Germany) using tetramethylsilane as an internal standard. Chemical shifts, δ , are given in parts per million (ppm), and spin multiplicities are given as s (singlet), br s (broad singlet), d (doublet), t (triplet), q (quartet) or m (multiplet). Coupling constants, J , are expressed in hertz (Hz). Melting points were recorded on a SMP10 Melting Point Apparatus (Stuart, Staffordshire, UK) and are uncorrected. Yields refer to isolated pure products and were not maximized. CHN analysis was performed on the ER-20 analyzer (Carlo-Erba, Val-de-Reuil, France). All compounds exhibited analytical and spectroscopic data that strongly agreed with their expected structures.

3.2. Synthesis of Compounds

The synthesis and characteristics of compounds are described below. The original NMR spectra are presented in the Supplementary Materials.

General Procedure for the Preparation of Derivatives 7a–k

A solution of tosyl chloride (190.65 mg, 1 mmol) in methylene chloride (5 mL) was added to a solution of NEt_3 (2 mmol) and aminoquinoline 5 (1 mmol) in methylene chloride (4 mL). The reaction mixture was stirred for 1 h at room temperature, diluted with 10 mL of water, and extracted with ethyl acetate (3×10 mL). The combined extracts were washed with brine, dried over anhydrous Na_2SO_4 , and evaporated under vacuum to give the required crude product that was recrystallized from isopropanol.

N-(2-(2,3-Dihydro-1H-cyclopenta[b]quinolin-9-ylamino)-ethyl)-4-methyl-benzenesulfonamide (7a). White solid; Yield 75%, m.p. 245–247 °C. $^1\text{H-NMR}$ (DMSO- d_6) δ : 2.17 (m, 2H, CH_2), 2.33 (s, 3H, CH_3), 2.80 (m, 2H, CH_2), 3.19 (m, 2H, CH_2), 3.83 (m, 4H, $2 \times \text{CH}_2$), 7.17 (d, 2H, $J = 8.4$ Hz, H_{ar}), 7.53 (t, 1H, $J = 7.2$ Hz, H_{ar}), 7.61 (d, 2H, $J = 8.4$ Hz, H_{ar}), 7.76 (t, 2H, $J = 7.3$ Hz, H_{ar}), 7.90 (m, 2H, NH, H_{ar}), 8.43 (m, 2H, NH, H_{ar}). Anal. Calcd for $\text{C}_{21}\text{H}_{23}\text{N}_3\text{O}_2\text{S}$: C, 66.12; H, 6.08; N, 11.01. Found: C, 66.18; H, 6.21; N, 11.12.

N-(3-(2,3-Dihydro-1H-cyclopenta[b]quinolin-9-ylamino)-propyl)-4-methyl-benzenesulfonamide (7b). White solid; Yield 72%, m.p. 213–215 °C. $^1\text{H-NMR}$ (DMSO- d_6 + CDCl_3) δ : 1.77 (m, 2H, CH_2), 2.12 (m, 2H, CH_2), 2.29 (s, 3H, CH_3), 2.83 (m, 2H, CH_2), 3.19 (m, 4H, $2 \times \text{CH}_2$), 3.75 (q, 2H, $J = 6.1$ Hz,

CH₂), 7.03 (d, 2H, *J* = 7.8 Hz, H_{ar}), 7.30 (m, 2H, NH, H_{ar}), 7.48 (m, 3H, NH, H_{ar}), 7.80 (d, 1H, *J* = 8.2 Hz, H_{ar}), 8.23 (m, 1H, NH), 8.25 (d, 1H, *J* = 8.6 Hz, H_{ar}). Anal. Calcd for C₂₂H₂₅N₃O₂S: C, 66.81, H, 6.37, N, 10.62. Found: C, 66.61, H, 6.47, N, 10.44.

N-(4-(2,3-Dihydro-1H-cyclopenta[b]quinolin-9-ylamino)-butyl)-4-methyl-benzenesulfonamide (7c). White solid; Yield 65%, m.p. 215–217 °C. ¹H-NMR (DMSO-d₆) δ: 1.51 (m, 2H, CH₂), 1.68 (m, 2H, CH₂), 2.20 (m, 2H, CH₂), 2.40 (s, 3H, CH₃), 2.75 (q, 2H, *J* = 6.2 Hz, CH₂), 3.26 (m, 4H, 2 × CH₂), 3.70 (q, 2H, *J* = 6.2 Hz, CH₂), 7.28 (d, 2H, *J* = 8.2 Hz, H_{ar}), 7.51 (m, 2H, NH, H_{ar}), 7.63 (d, 2H, *J* = 8.4 Hz, H_{ar}), 7.76 (t, 1H, *J* = 7.4 Hz, H_{ar}), 7.95 (d, 1H, *J* = 8.2 Hz, H_{ar}), 8.54 (d, 1H, *J* = 8.2 Hz, H_{ar}), 8.80 (t, 1H, *J* = 6.2 Hz, NH). Anal. Calcd for C₂₃H₂₇N₃O₂S: C, 67.45, H, 6.65, N, 10.26. Found: C, 67.57, H, 6.61, N, 10.41.

N-(5-(2,3-Dihydro-1H-cyclopenta[b]quinolin-9-ylamino)-pentyl)-4-methyl-benzenesulfonamide (7d). White solid; Yield 76%, m.p. 173–175 °C. ¹H-NMR (DMSO-d₆) δ: 1.57 (m, 6H, 3 × CH₂), 2.19 (m, 2H, CH₂), 2.38 (s, 3H, CH₃), 2.75 (q, 2H, *J* = 6.3 Hz, CH₂), 3.26 (m, 4H, 2 × CH₂), 3.67 (q, 2H, *J* = 6.3 Hz, CH₂), 7.25 (d, 2H, *J* = 8.2 Hz, H_{ar}), 7.47 (m, 2H, NH, H_{ar}), 7.62 (d, 2H, *J* = 8.2 Hz, H_{ar}), 7.76 (t, 1H, *J* = 7.3 Hz, H_{ar}), 7.93 (d, 1H, *J* = 8.2 Hz, H_{ar}), 8.49 (d, 1H, *J* = 8.2 Hz, H_{ar}), 8.76 (t, 1H, *J* = 6.2 Hz, NH). Anal. Calcd for C₂₄H₂₉N₃O₂S: C, 68.05, H, 6.90, N, 9.92. Found: C, 68.29, H, 6.77, N, 9.78.

N-(6-(2,3-Dihydro-1H-cyclopenta[b]quinolin-9-ylamino)-hexyl)-4-methyl-benzenesulfonamide (7e). White solid; Yield 73%, m.p. 230–232 °C. ¹H-NMR (DMSO-d₆) δ: 1.57 (m, 6H, 4 × CH₂), 2.20 (m, 2H, CH₂), 2.39 (s, 3H, CH₃), 2.78 (q, 2H, *J* = 6.2 Hz, CH₂), 3.20 (m, 2H, CH₂), 3.30 (m, 2H, CH₂), 3.72 (q, 2H, *J* = 6.2 Hz, CH₂), 7.23 (d, 2H, *J* = 8.2 Hz, H_{ar}), 7.44 (m, 2H, NH, H_{ar}), 7.58 (d, 2H, *J* = 8.2 Hz, H_{ar}), 7.73 (t, 1H, *J* = 7.3 Hz, H_{ar}), 8.00 (d, 1H, *J* = 8.2 Hz, H_{ar}), 8.33 (d, 1H, *J* = 8.2 Hz, H_{ar}), 8.73 (t, 1H, *J* = 6.2 Hz, NH). Anal. Calcd for C₂₅H₃₁N₃O₂S: C, 68.62, H, 7.14, N, 9.60. Found: C, 68.90, H, 7.27, N, 9.44.

4-Methyl-*N*-(3-(1,2,3,4-tetrahydro-acridin-9-ylamino)-propyl)-benzenesulfonamide (7f). White solid; Yield 68%, m.p. 222–224 °C. ¹H-NMR (DMSO-d₆) δ: 1.88 (m, 6H, 3 × CH₂), 2.38 (s, 3H, CH₃), 2.67 (m, 2H, CH₂), 2.80 (q, 2H, *J* = 6.2 Hz, CH₂), 3.07 (m, 2H, CH₂), 3.90 (q, 2H, *J* = 5.6 Hz, CH₂), 7.28 (d, 2H, *J* = 8.2 Hz, H_{ar}), 7.51 (t, 1H, *J* = 7.7 Hz, H_{ar}), 7.63 (d, 2H, *J* = 8.2 Hz, H_{ar}), 7.79 (m, 3H, 2 × NH, H_{ar}), 8.08 (d, 1H, *J* = 8.5 Hz, H_{ar}), 8.39 (d, 1H, *J* = 8.5 Hz, H_{ar}). Anal. Calcd for C₂₃H₂₇N₃O₂S: C, 67.45, H, 6.65, N, 10.26. Found: C, 67.66, H, 6.70, N, 10.22.

4-Methyl-*N*-(4-(1,2,3,4-tetrahydro-acridin-9-ylamino)-butyl)-benzenesulfonamide (7g). White solid; Yield 71%, m.p. 165–167 °C. ¹H-NMR (CDCl₃) δ: 1.69 (m, 4H, 2 × CH₂), 1.84 (m, 4H, 2 × CH₂), 2.38 (s, 3H, CH₃), 2.62 (m, 2H, CH₂), 2.95 (m, 2H, CH₂), 3.07 (m, 2H, CH₂), 3.58 (q, 2H, *J* = 6.6 Hz, CH₂), 4.77 (m, 1H, NH), 5.45 (m, 1H, NH), 7.23 (d, 2H, *J* = 7.8 Hz, H_{ar}), 7.31 (m, 1H, H_{ar}), 7.53 (m, 1H, H_{ar}), 7.74 (d, 2H, *J* = 8.4 Hz, H_{ar}), 7.95 (d, 1H, *J* = 8.8 Hz, H_{ar}), 8.02 (d, 1H, *J* = 8.2 Hz, H_{ar}). Anal. Calcd for C₂₄H₂₉N₃O₂S: C, 68.05, H, 6.90, N, 9.92. Found: C, 68.31, H, 6.72, N, 9.81.

4-Methyl-*N*-(5-(1,2,3,4-tetrahydro-acridin-9-ylamino)-pentyl)-benzenesulfonamide (7h). White solid; Yield 73%, m.p. 235–237 °C. ¹H-NMR (CDCl₃) δ: 1.69 (m, 6H, 3 × CH₂), 1.97 (m, 4H, 2 × CH₂), 2.36 (s, 3H, CH₃), 2.63 (m, 2H, CH₂), 2.94 (m, 2H, CH₂), 3.08 (m, 2H, CH₂), 3.56 (q, 2H, *J* = 6.7 Hz, CH₂), 4.75 (m, 1H, NH), 5.45 (m, 1H, NH), 7.24 (d, 2H, *J* = 7.8 Hz, H_{ar}), 7.28 (m, 1H, H_{ar}), 7.53 (t, 1H, *J* = 7.1 Hz, H_{ar}), 7.74 (d, 2H, *J* = 8.5 Hz, H_{ar}), 7.96 (d, 1H, *J* = 8.8 Hz, H_{ar}), 8.04 (d, 1H, *J* = 8.3 Hz, H_{ar}). Anal. Calcd for C₂₅H₃₁N₃O₂S: C, 68.62, H, 7.14, N, 9.60. Found: C, 68.76, H, 7.32, N, 9.52.

4-Methyl-*N*-(3-(7,8,9,10-tetrahydro-6H-cyclohepta[b]quinolin-11-ylamino)-propyl)-benzenesulfonamide (7i). White solid; Yield 65%, m.p. 213–215 °C. ¹H-NMR (DMSO-d₆) δ: 1.64 (m, 2H, CH₂), 1.85 (m, 6H, 3 × CH₂), 2.35 (s, 3H, CH₃), 2.76 (q, 2H, *J* = 6.1 Hz, CH₂), 2.88 (m, 2H, CH₂), 3.23 (m, 2H, CH₂), 3.72 (m, 2H, CH₂), 7.31 (d, 2H, *J* = 8.3 Hz, CH₂), 7.58 (d, 2H, *J* = 8.3 Hz, H_{ar}), 7.71 (m, 3H, 2 × NH, H_{ar}), 7.88 (t, 1H, *J* = 8.1 Hz, H_{ar}), 8.06 (d, 1H, *J* = 8.3 Hz, H_{ar}), 8.42 (d, 1H, *J* = 8.3 Hz, H_{ar}). Anal. Calcd for C₂₄H₂₉N₃O₂S: C, 68.05, H, 6.90, N, 9.92. Found: C, 68.30, H, 6.72, N, 9.91.

4-Methyl-*N*-(4-(7,8,9,10-tetrahydro-6H-cyclohepta[b]quinolin-11-ylamino)-butyl)-benzenesulfonamide (7j). White solid; Yield 66%, m.p. 235–237 °C. ¹H-NMR (CDCl₃) δ: 1.60 (m, 4H, 2 × CH₂), 1.81 (m, 6H, 3 × CH₂), 2.39 (s, 3H, CH₃), 2.63 (m, 2H, CH₂), 2.95 (m, 2H, CH₂), 3.15 (m, 2H, CH₂), 3.92 (m, 2H, CH₂), 7.27 (m, 2H, H_{ar}), 7.57 (t, 1H, *J* = 7.6 Hz, H_{ar}), 7.78 (d, 2H, *J* = 8.3 Hz, H_{ar}), 7.80 (m, 1H, H_{ar}), 8.23 (d,

1H, $J = 8.3$ Hz, H_{ar}), 8.30 (d, 1H, $J = 8.3$ Hz, H_{ar}). Anal. Calcd for $C_{25}H_{31}N_3O_2S$: C, 68.62, H, 7.14, N, 9.60. Found: C, 68.66, H, 7.01, N, 9.76.

N-(3-(6,7,8,9,10,11-Hexahydro-cycloocta[*b*]quinolin-12-ylamino)-propyl)-4-methyl-benzenesulfonamide (7k). White solid; Yield 65%, m.p. 210–212 °C. 1H -NMR (DMSO- d_6) δ : 1.36 (m, 2H, CH_2), 1.53 (m, 2H, CH_2), 1.71 (m, 2H, CH_2), 1.94 (m, 4H, $2 \times CH_2$), 2.41 (s, 3H, CH_3), 2.84 (q, 2H, $J = 6.1$ Hz, CH_2), 2.95 (m, 2H, CH_2), 3.25 (m, 2H, CH_2), 3.92 (m, 2H, CH_2), 7.27 (d, 2H, $J = 8.2$ Hz, H_{ar}), 7.52 (m, 1H, H_{ar}), 7.66 (d, 2H, $J = 8.4$ Hz, H_{ar}), 7.78 (m, 3H, $2 \times NH$, H_{ar}), 8.33 (m, 2H, H_{ar}). Anal. Calcd for $C_{25}H_{31}N_3O_2S$: C, 68.62, H, 7.14, N, 9.60. Found: C, 68.43, H, 7.07, N, 9.84.

3.3. Biological Assays

3.3.1. Enzymatic Assays

- In vitro AChE, BChE and CES Inhibition

All experiments were carried out in accordance with the standard protocols approved by IPAC RAS. Human erythrocyte AChE, equine serum BChE, porcine liver CES, acetylthiocholine iodide (ATCh), butyrylthiocholine iodide (BTCh), 5,5'-dithio-bis-(2-nitrobenzoic acid) (DTNB), and 4-nitrophenol acetate (4-NPA) were purchased from Sigma-Aldrich (Saint Louis, MO, USA).

AChE and BChE activities were measured by the colorimetric method of Ellman et al. [94]. The assay solution consisted of 0.1 M K/Na phosphate buffer pH 7.5, 25 °C, 0.33 mM DTNB, 0.02 unit/mL AChE or BChE, and 1 mM substrate (ATCh or BTCh, respectively). Reagent blanks consisted of reaction mixtures without substrates.

The activity of CES was determined spectrophotometrically at 405 nm to monitor the release of 4-nitrophenol [95] in 0.1 M K/Na phosphate buffer pH 8.0, 25 °C. Final enzyme and substrate (4-nitrophenyl acetate) concentrations were 0.02 unit/mL and 1 mM, respectively. Assays were carried out with a blank containing all constituents except porcine CES to assess non-enzymatic hydrolysis.

Test compounds were dissolved in DMSO; reaction mixtures contained 2% (*v/v*) of the solvent, a concentration shown not to affect the activity of the enzymes on its own (data not shown). Tacrine, donepezil, and bis-4-nitrophenyl phosphate (BNPP), a selective CES inhibitor, were used as positive controls.

An initial evaluation of inhibitory activity of compounds was carried out by determination of the AChE, BChE and CES inhibition at a compound concentration of 20 μ M. For this, a sample of the corresponding enzyme was incubated with the test compound for 5 min at 25 °C for temperature equilibration; then the enzyme residual activity was determined. Each experiment was performed in triplicate.

For the most active compounds, the IC_{50} values (the concentration of inhibitor required to decrease the enzyme activity by 50%) were determined. Eight different concentrations of the test compounds in the range 10^{-12} – 10^{-4} M were selected in order to obtain inhibition of esterase activity between 20% and 80%. The test compounds were added to the assay solution and incubated with the enzyme at 25 °C for 5 min (for temperature equilibration) followed by the addition of substrate. A parallel control was made for the assay solution with no inhibitor.

Measurements were performed in the FLUOStar OPTIMA microplate spectrophotometer (BMG Labtech, Ortenberg, Germany). Each experiment for the IC_{50} assay was performed in triplicate. The results were expressed as the mean \pm SEM. The reaction rates in the presence and absence of inhibitor were compared, and the percent residual enzyme activity due to the presence of test compounds was calculated. IC_{50} values were determined graphically from inhibition curves (log inhibitor concentration vs. percent residual enzyme activity) using Origin 6.1 software (OriginLab, Northampton, MA, USA).

- Kinetic Study of AChE and BChE Inhibition. Determination of Steady-State Inhibition Constants

Mechanisms of AChE and BChE inhibition were assessed via a thorough analysis of enzyme kinetics. Residual activity was measured following 5 min incubation at 25 °C (for temperature equilibration) with three increasing concentrations of inhibitor and six decreasing substrate concentrations. Substrate was added immediately after the 5 min incubation with inhibitor and the rates of absorption were monitored at 412 nm using the FLUOStar OPTIMA (BMG Labtech) microplate spectrophotometer. Inhibition constants K_i (competitive component) and αK_i (noncompetitive component) were determined by linear regression of $1/V$ versus $1/[S]$ double-reciprocal (Lineweaver-Burk) plots using Origin 6.1 software. Data were expressed as mean \pm SEM ($n = 3$ experiments).

3.3.2. Propidium Displacement Studies

The ability of the test compounds to competitively displace propidium, a selective ligand of the PAS of AChE, was evaluated by the fluorescence method [93,96]. *Ee*AChE was used owing to its high degree of purification, high activity, and lower cost than human AChE (hAChE). In addition, we performed 3D alignment of the crystal structures of *Ee*AChE (PDB: 1C2O) and hAChE (PDB: 4EY7) using YASARA-Structure 18.4.24 for Windows, which showed that the two structures were essentially congruent with an RMSD of 0.623 Å over 527 aligned residues and 88.6% sequence identity. The fluorescence intensity of propidium iodide bound with AChE increases several times; decreasing fluorescence intensity of the bound propidium in the presence of the test compounds shows their ability to bind to the PAS of AChE [24,27].

To determine the degree of displacement (% displacement) of propidium from the PAS of AChE, *Ee*AChE (final concentration, 7 μ M) was incubated with the test compound at a concentration of 20 μ M in 1 mM Tris-HCl buffer pH 8.0, 25 °C, for 15 min. Then, propidium iodide solution (final concentration, 8 μ M) was added, the samples were incubated for 15 min and the fluorescence spectrum (530 nm (excitation) and 600 nm (emission)) was taken. Donepezil and tacrine were used as reference compounds. The blank contained propidium iodide of the same concentration in 1 mM Tris-HCl buffer pH 8.0. The measurements were carried out in triplicate on the FLUOStar Optima microplate reader (BMG Labtech), and the results were calculated by the following formula:

$$\% \text{ Displacement} = 100 - (\text{IF}_{\text{AChE} + \text{Propidium} + \text{inhibitor}} / \text{IF}_{\text{AChE} + \text{Propidium}}) \times 100 \quad (1)$$

where $\text{IF}_{\text{AChE} + \text{Propidium}}$ is the fluorescence intensity of the propidium associated with AChE in the absence of the test compound (taken as 100%), and $\text{IF}_{\text{AChE} + \text{Propidium} + \text{inhibitor}}$ is the fluorescence intensity of the propidium associated with AChE in the presence of the test compound.

3.3.3. Antioxidant Activity: ABTS Radical Cation Scavenging Activity Assay

Radical scavenging activity of the compounds was assessed using the ABTS radical decolorization assay [97] with some modifications [50]. ABTS was purchased from Tokyo Chemical Industry Co. (Tokyo, Japan), potassium persulfate (dipotassium peroxodisulfate), Trolox[®] (6-hydroxy-2,5,7,8-tetramethylchroman-2-carboxylic acid), and HPLC grade ethanol were obtained from Sigma-Aldrich. Aqueous solutions were prepared using deionized water.

The solution of cation radical $\text{ABTS}^{\bullet+}$ was produced by incubation of ABTS with potassium persulfate in deionized water for 12–16 h at room temperature in the dark. Radical scavenging capacity of the compounds was analyzed by mixing 10 μ L of compound with 240 μ L of $\text{ABTS}^{\bullet+}$ working solution in ethanol (100 μ M final concentration). After 1 h of incubation, the reduction in absorbance was measured spectrophotometrically at 734 nm using the xMark microplate UV/VIS microplate spectrophotometer (Bio-Rad, Hercules, CA, USA). Ethanol blanks were run in each assay. Values were obtained from three replicates of each sample and three independent experiments. Trolox was used as the antioxidant standard.

The antioxidant activity is reported as Trolox equivalent antioxidant capacity (TEAC values) by comparing ($A_0 - A_{\text{test}}$) of the test antioxidant with ($A_0 - A_{\text{Trolox}}$) of the Trolox standard at a concentration of 20 μM after a reaction time of 1 h. A_0 is the absorbance of a control lacking any radical scavenger and $A_{\text{test/Trolox}}$ is the absorbance of the remaining ABTS^{•+} in the presence of the test compound or Trolox, respectively:

$$\text{TEAC} = (A_0 - A_{\text{test}})/(A_0 - A_{\text{Trolox}}) \quad (2)$$

3.4. Molecular Modeling Studies

X-ray structures of human AChE in *apo*-form and co-crystallized with different ligands (PDB: 4EY4–4EY7) [98] and an optimized X-ray structure of human BChE (PDB: 1P0I) [99,100] were used for molecular docking. Ligand structures were optimized using a DFT quantum chemistry method (B3LYP/6-31G*, GAMESS-US [101] software). Partial atomic charges on ligand atoms were assigned from QM data according to the Löwdin scheme [102]. Molecular docking was performed with AutoDock 4.2.6 software [103]. The grid box for docking included the entire active site gorge of AChE (22.5 Å × 22.5 Å × 22.5 Å grid box dimensions) and BChE (15 Å × 20.25 Å × 18 Å grid box dimensions) with a grid spacing of 0.375 Å. The main Lamarckian Genetic Algorithm (LGA) [104] parameters were 256 runs, 25×10^6 evaluations, 27×10^4 generations, and a population size of 3000. Figures were prepared with PyMOL (www.pymol.org).

3.5. Prediction of ADMET Profiles and PAINS Analysis

Human intestinal absorption (HIA) [105], blood-brain barrier permeability (LogBB) [106], and hERG-mediated cardiac toxicity risk (channel affinity pK_i and inhibitory activity pIC_{50}) [107] were estimated using the integrated online service for ADMET properties prediction (ADMET Prediction Service) [108]. It implements the predictive QSAR models based on accurate and representative training sets, fragmental descriptors, and artificial neural networks. The lipophilicity (LogPow) and aqueous solubility (pS) were estimated by the ALogPS 3.0 neural network model implemented in the OCHEM platform [109]. The quantitative estimate of drug-likeness (QED) values [110] were calculated and the Pan Assay INterference compoundS (PAINS) alerts were checked using the RDKit version 2019.03.4 software [111].

3.6. Statistical Analyses

Results are presented as mean \pm SEM calculated using GraphPad Prism version 6.05 (San Diego, CA, USA) for Windows. Plots, linear regressions, and IC_{50} values were determined using Origin 6.1 (Northampton, MA, USA) for Windows.

4. Conclusions

New hybrids of 4-amino-2,3-polymethylene-quinoline and *p*-tolylsulfonamide with different aliphatic ring sizes and alkylene spacers of increasing length were synthesized and their structures established. All synthesized compounds exhibited high dual anticholinesterase activity and greater selectivity toward BChE. They possessed low anti-CES activity, suggesting the absence of potential unwanted drug-drug interactions in prospective clinical use.

Kinetics studies were consistent with mixed-type reversible inhibition. Molecular docking into AChE and BChE provided detailed insights into the binding modes demonstrating dual-site binding of the conjugates in AChE and clarifying differences in the structure-activity relationships for AChE and BChE inhibition.

The conjugates had the ability to bind to the AChE PAS and displace propidium, indicating their potential to block AChE-induced β -amyloid aggregation, thereby potentially exerting disease-modifying capability. All compounds demonstrated low antioxidant activity.

Computational ADMET profiles predicted that all the conjugates should have good intestinal absorption, medium blood-brain barrier permeability, and medium cardiac toxicity risks. Moreover, the PAINS filter check for the compounds did not identify any alerts.

Overall, the developed hybrid compounds demonstrated potent dual anticholinesterase activity along with the predicted propensity to block AChE-induced aggregation of β -amyloid. Thus, they have the potential for treating symptoms as well as exerting disease-modifying effects and show promise for further development and optimization as multitarget anti-AD agents. In particular, the lead compound 4-methyl-N-(5-(1,2,3,4-tetrahydro-acridin-9-ylamino)-pentyl)benzenesulfonamide (**7h**), with an unmodified six-membered tacrine ring and $m = 5$, exhibited maximum anti-AChE activity with $IC_{50} = 0.131 \pm 0.01 \mu\text{M}$ (five times more potent than tacrine) and high anti-BChE activity. It is a mixed-type AChE inhibitor with the highest percentage of propidium displacement, very good intestinal absorption and medium predicted blood-brain barrier permeability.

Supplementary Materials: The following are available online: Figures S1–S11: NMR spectra for **7a–k**.

Author Contributions: Conceptualization, G.F.M., N.P.B., S.V.L. and A.N.P.; Formal analysis, S.V.L., T.Y.A., E.V.R. (Eugene V. Radchenko), V.A.P. and R.J.R.; Investigation, N.V.K., N.P.B., S.V.L., E.V.R. (Elena V. Rudakova), A.N.P., I.V.S., E.V.R. (Eugene V. Radchenko), V.A.P. and R.J.R.; Methodology, G.F.M., N.P.B., S.V.L., T.Y.A. and A.N.P.; Software, S.V.L., T.Y.A., E.V.R. (Eugene V. Radchenko), V.A.P. and R.J.R.; Supervision, G.F.M. and S.O.B.; Visualization, S.V.L., T.Y.A., E.V.R. (Eugene V. Radchenko), V.A.P. and R.J.R.; Writing—original draft, N.V.K., N.P.B., S.V.L., A.N.P. and E.V.R. (Eugene V. Radchenko); Writing—review & editing, G.F.M., N.V.K., N.P.B., E.V.R. (Eugene V. Radchenko) and R.J.R. All authors have read and agreed to the published version of the manuscript.

Funding: This research was partly supported by grant #19-53-26016_a of the Russian Foundation for Basic Research and by the IPAC RAS State Targets Project # 0090-2019-0005. Support for RJR's contributions was provided by the University of Michigan. The funding sources had no role in the study design; collection, analysis and interpretation of data; writing of the manuscript; or the decision to submit the article for publication.

Acknowledgments: We would like to thank the shared research facilities of the HPC computing resources at Lomonosov Moscow State University [112] for the use of equipment for computer modeling and the “Centre for Collective Use of IPAC RAS” for use of equipment cited in the Methods.

Conflicts of Interest: The authors declare no conflict of interest.

References

1. Alzheimer's Association. 2015 Alzheimer's disease facts and figures. *Alzheimer Dement.* **2015**, *11*, 332–384. [[CrossRef](#)] [[PubMed](#)]
2. Huang, Y.; Mucke, L. Alzheimer mechanisms and therapeutic strategies. *Cell* **2012**, *148*, 1204–1222. [[CrossRef](#)] [[PubMed](#)]
3. Carreiras, M.C.; Mendes, E.; Perry, M.J.; Francisco, A.P.; Marco-Contelles, J. The multifactorial nature of Alzheimer's disease for developing potential therapeutics. *Curr. Top. Med. Chem.* **2013**, *13*, 1745–1770. [[CrossRef](#)] [[PubMed](#)]
4. Querfurth, H.W.; LaFerla, F.M. Alzheimer's disease. *N. Engl. J. Med.* **2010**, *362*, 329–344. [[CrossRef](#)] [[PubMed](#)]
5. Huang, W.J.; Zhang, X.; Chen, W.W. Role of oxidative stress in Alzheimer's disease. *Biomed. Rep.* **2016**, *4*, 519–522. [[CrossRef](#)] [[PubMed](#)]
6. Scarpini, E.; Schelterns, P.; Feldman, H. Treatment of Alzheimer's disease; current status and new perspectives. *Lancet Neurol.* **2003**, *2*, 539–547. [[CrossRef](#)]
7. Perry, E.K.; Tomlinson, B.E.; Blessed, G.; Bergmann, K.; Gibson, P.H.; Perry, R.H. Correlation of cholinergic abnormalities with senile plaques and mental test scores in senile dementia. *Br. Med. J.* **1978**, *2*, 1457–1459. [[CrossRef](#)] [[PubMed](#)]
8. Agatonovic-Kustrin, S.; Kettle, C.; Morton, D.W. A molecular approach in drug development for Alzheimer's disease. *Biomed. Pharmacother.* **2018**, *106*, 553–565. [[CrossRef](#)]
9. Birks, J. Cholinesterase inhibitors for Alzheimer's disease. *Cochrane Database Syst. Rev.* **2006**. [[CrossRef](#)]
10. Mangialasche, F.; Solomon, A.; Winblad, B.; Mecocci, P.; Kivipelto, M. Alzheimer's disease: Clinical trials and drug development. *Lancet Neurol.* **2010**, *9*, 702–716. [[CrossRef](#)]
11. Allgaier, M.; Allgaier, C. An update on drug treatment options of Alzheimer's disease. *Front. Biosci.* **2014**, *19*, 1345–1354. [[CrossRef](#)]

12. Reid, G.A.; Chilukuri, N.; Darvesh, S. Butyrylcholinesterase and the cholinergic system. *Neuroscience* **2013**, *234*, 53–68. [[CrossRef](#)]
13. Giacobini, E. Cholinesterases: New roles in brain function and in Alzheimer's disease. *Neurochem. Res.* **2003**, *28*, 515–522. [[CrossRef](#)] [[PubMed](#)]
14. Martinez, A.; Castro, A. Novel cholinesterase inhibitors as future effective drugs for the treatment of Alzheimer's disease. *Expert Opin. Investig. Drugs* **2006**, *15*, 1–12. [[CrossRef](#)] [[PubMed](#)]
15. Mesulam, M.M.; Geula, C. Butyrylcholinesterase reactivity differentiates the amyloid plaques of aging from those of dementia. *Ann. Neurol.* **1994**, *36*, 722–727. [[CrossRef](#)]
16. Ballard, C.; Greig, N.; Guillozet-Bongaarts, A.; Enz, A.; Darvesh, S. Cholinesterases: Roles in the Brain during Health and Disease. *Curr. Alzheimer. Res.* **2005**, *2*, 307–318. [[CrossRef](#)] [[PubMed](#)]
17. Greig, N.H.; Utsuki, T.; Ingram, D.K.; Wang, Y.; Pepeu, G.; Scali, C.; Yu, Q.S.; Mamczarz, J.; Holloway, H.W.; Giordano, T.; et al. Selective butyrylcholinesterase inhibition elevates brain acetylcholine, augments learning and lowers Alzheimer beta-amyloid peptide in rodent. *Proc. Natl. Acad. Sci. USA* **2005**, *102*, 17213–17218. [[CrossRef](#)] [[PubMed](#)]
18. Furukawa-Hibi, Y.; Alkam, T.; Nitta, A.; Matsuyama, A.; Mizoguchi, H.; Suzuki, K.; Moussaoui, S.; Yu, Q.S.; Greig, N.H.; Nagai, T.; et al. Butyrylcholinesterase inhibitors ameliorate cognitive dysfunction induced by amyloid-beta peptide in mice. *Behav. Brain Res.* **2011**, *225*, 222–229. [[CrossRef](#)]
19. Lane, R.M.; Potkin, S.G.; Enz, A. Targeting acetylcholinesterase and butyrylcholinesterase in dementia. *Int. J. Neuropsychopharmacol.* **2006**, *9*, 101–124. [[CrossRef](#)]
20. Nordberg, A.; Ballard, C.; Bullock, R.; Darreh-Shori, T.; Somogyi, M. A review of butyrylcholinesterase as a therapeutic target in the treatment of Alzheimer's disease. *Prim. Care Companion CNS Disord.* **2013**, *15*. [[CrossRef](#)]
21. Kosak, U.; Brus, B.; Knez, D.; Sink, R.; Zakej, S.; Trontelj, J.; Pisljar, A.; Slenc, J.; Gobec, M.; Zivin, M.; et al. Development of an in-vivo active reversible butyrylcholinesterase inhibitor. *Sci. Rep.* **2016**, *6*, 39495. [[CrossRef](#)] [[PubMed](#)]
22. Bartorelli, L.; Giraldi, C.; Saccardo, M.; Cammarata, S.; Bottini, G.; Fasanaro, A.M.; Trequattrini, A. Effects of switching from an AChE inhibitor to a dual AChE-BuChE inhibitor in patients with Alzheimer's disease. *Curr. Med. Res. Opin.* **2005**, *21*, 1809–1817. [[CrossRef](#)] [[PubMed](#)]
23. Moran, M.A.; Mufson, E.J.; Gomez-Ramos, P. Cholinesterases colocalize with sites of neurofibrillary degeneration in aged and Alzheimer's brains. *Acta Neuropathol.* **1994**, *87*, 284–292. [[CrossRef](#)] [[PubMed](#)]
24. De Ferrari, G.V.; Canales, M.A.; Shin, I.; Weiner, L.M.; Silman, I.; Inestrosa, N.C. A structural motif of acetylcholinesterase that promotes amyloid beta-peptide fibril formation. *Biochemistry* **2001**, *40*, 10447–10457. [[CrossRef](#)] [[PubMed](#)]
25. Darvesh, S.; Cash, M.K.; Reid, G.A.; Martin, E.; Mitnitski, A.; Geula, C. Butyrylcholinesterase is associated with beta-amyloid plaques in the transgenic APPSWE/PSEN1dE9 mouse model of Alzheimer disease. *J. Neuropathol. Exp. Neurol.* **2012**, *71*, 2–14. [[CrossRef](#)]
26. Bartolini, M.; Bertucci, C.; Cavrini, V.; Andrisano, V. β -Amyloid aggregation induced by human acetylcholinesterase: Inhibition studies. *Biochem. Pharmacol.* **2003**, *65*, 407–416. [[CrossRef](#)]
27. Inestrosa, N.C.; Dinamarca, M.C.; Alvarez, A. Amyloid-cholinesterase interactions. Implications for Alzheimer's disease. *FEBS J.* **2008**, *275*, 625–632. [[CrossRef](#)]
28. Arce, M.P.; Rodriguez-Franco, M.I.; Gonzalez-Munoz, G.C.; Perez, C.; Lopez, B.; Villarroya, M.; Lopez, M.G.; Garcia, A.G.; Conde, S. Neuroprotective and cholinergic properties of multifunctional glutamic acid derivatives for the treatment of Alzheimer's disease. *J. Med. Chem.* **2009**, *52*, 7249–7257. [[CrossRef](#)]
29. Lushchekina, S.V.; Kots, E.D.; Novichkova, D.A.; Petrov, K.A.; Masson, P. Role of Acetylcholinesterase in β -Amyloid Aggregation Studied by Accelerated Molecular Dynamics. *BioNanoScience* **2017**, *7*, 396–402. [[CrossRef](#)]
30. Inestrosa, N.C.; Alvarez, A.; Pérez, C.A.; Moreno, R.D.; Vicente, M.; Linker, C.; Casanueva, O.I.; Soto, C.; Garrido, J. Acetylcholinesterase Accelerates Assembly of Amyloid- β -Peptides into Alzheimer's Fibrils: Possible Role of the Peripheral Site of the Enzyme. *Neuron* **1996**, *16*, 881–891. [[CrossRef](#)]
31. Muñoz-Ruiz, P.; Rubio, L.; García-Palomero, E.; Dorronsoro, I.; del Monte-Millán, M.; Valenzuela, R.; Usán, P.; de Austria, C.; Bartolini, M.; Andrisano, V.; et al. Design, Synthesis, and Biological Evaluation of Dual Binding Site Acetylcholinesterase Inhibitors: New Disease-Modifying Agents for Alzheimer's Disease. *J. Med. Chem.* **2005**, *48*, 7223–7233. [[CrossRef](#)] [[PubMed](#)]

32. Camps, P.; Formosa, X.; Galdeano, C.; Gomez, T.; Munoz-Torrero, D.; Ramirez, L.; Viayna, E.; Gomez, E.; Isambert, N.; Lavilla, R.; et al. Tacrine-based dual binding site acetylcholinesterase inhibitors as potential disease-modifying anti-Alzheimer drug candidates. *Chem. Biol. Interact.* **2010**, *187*, 411–415. [[CrossRef](#)] [[PubMed](#)]
33. Zueva, I.; Dias, J.; Lushchekina, S.; Semenov, V.; Mukhamedyarov, M.; Pashirova, T.; Babaev, V.; Nachon, F.; Petrova, N.; Nurullin, L.; et al. New evidence for dual binding site inhibitors of acetylcholinesterase as improved drugs for treatment of Alzheimer's disease. *Neuropharmacology* **2019**, *155*, 131–141. [[CrossRef](#)] [[PubMed](#)]
34. Darvesh, S. Butyrylcholinesterase as a diagnostic and therapeutic target for Alzheimer's disease. *Curr. Alzheimer. Res.* **2016**, *13*, 1–5. [[CrossRef](#)]
35. Ramanan, V.K.; Risacher, S.L.; Nho, K.; Kim, S.; Swaminathan, S.; Shen, L.; Foroud, T.M.; Hakonarson, H.; Huentelman, M.J.; Aisen, P.S.; et al. APOE and BCHE as modulators of cerebral amyloid deposition: A florbetapir PET genome-wide association study. *Mol. Psychiatry* **2014**, *19*, 351–357. [[CrossRef](#)] [[PubMed](#)]
36. Bajda, M.; Guzior, N.; Ignasik, M.; Malawska, B. Multi-target-directed ligands in Alzheimer's disease treatment. *Curr. Med. Chem.* **2011**, *18*, 4949–4975. [[CrossRef](#)]
37. Oset-Gasque, M.J.; Marco-Contelles, J. Alzheimer's Disease, the "One-Molecule, One-Target" Paradigm, and the Multitarget Directed Ligand Approach. *ACS Chem. Neurosci.* **2018**, *9*, 401–403. [[CrossRef](#)]
38. De Freitas Silva, M.; Dias, K.S.T.; Gontijo, V.S.; Ortiz, C.J.C.; Viegas, C., Jr. Multi-Target Directed Drugs as a Modern Approach for Drug Design Towards Alzheimer's Disease: An Update. *Curr. Med. Chem.* **2018**, *25*, 3491–3525. [[CrossRef](#)]
39. Savelieff, M.G.; Nam, G.; Kang, J.; Lee, H.J.; Lee, M.; Lim, M.H. Development of multifunctional molecules as potential therapeutic candidates for Alzheimer's disease, Parkinson's disease, and amyotrophic lateral sclerosis in the last decade. *Chem. Rev.* **2019**, *119*, 1221–1322. [[CrossRef](#)]
40. Cavalli, A.; Bolognesi, M.L.; Minarini, A.; Rosini, M.; Tumiatti, V.; Recanatini, M.; Melchiorre, C. Multi-target-directed ligands to combat neurodegenerative diseases. *J. Med. Chem.* **2008**, *51*, 347–372. [[CrossRef](#)]
41. Ismaili, L.; Refouvelet, B.; Benchekroun, M.; Brogi, S.; Brindisi, M.; Gemma, S.; Campiani, G.; Filipic, S.; Agbaba, D.; Esteban, G.; et al. Multitarget compounds bearing tacrine- and donepezil-like structural and functional motifs for the potential treatment of Alzheimer's disease. *Prog. Neurobiol.* **2017**, *151*, 4–34. [[CrossRef](#)] [[PubMed](#)]
42. Li, Q.; He, S.; Chen, Y.; Feng, F.; Qu, W.; Sun, H. Donepezil-based multi-functional cholinesterase inhibitors for treatment of Alzheimer's disease. *Eur. J. Med. Chem.* **2018**, *158*, 463–477. [[CrossRef](#)] [[PubMed](#)]
43. Mishra, P.; Kumar, A.; Panda, G. Anti-cholinesterase hybrids as multi-target-directed ligands against Alzheimer's disease (1998–2018). *Bioorg. Med. Chem.* **2019**, *27*, 895–930. [[CrossRef](#)] [[PubMed](#)]
44. Mesiti, F.; Chavarria, D.; Gaspar, A.; Alcaro, S.; Borges, F. The chemistry toolbox of multitarget-directed ligands for Alzheimer's disease. *Eur. J. Med. Chem.* **2019**, *181*, 111572. [[CrossRef](#)]
45. Rosini, M.; Simoni, E.; Bartolini, M.; Soriano, E.; Marco-Contelles, J.; Andrisano, V.; Monti, B.; Windisch, M.; Hutter-Paier, B.; McClymont, D.W.; et al. The bivalent ligand approach as a tool for improving the in vitro anti-Alzheimer multitarget profile of dimebon. *ChemMedChem* **2013**, *8*, 1276–1281. [[CrossRef](#)]
46. Sameem, B.; Saeedi, M.; Mahdavi, M.; Shafiee, A. A review on tacrine-based scaffolds as multi-target drugs (MTDLs) for Alzheimer's disease. *Eur. J. Med. Chem.* **2017**, *128*, 332–345. [[CrossRef](#)]
47. Rosini, M.; Simoni, E.; Bartolini, M.; Tarozzi, A.; Matera, R.; Milelli, A.; Hrelia, P.; Andrisano, V.; Bolognesi, M.L.; Melchiorre, C. Exploiting the lipoic acid structure in the search for novel multitarget ligands against Alzheimer's disease. *Eur. J. Med. Chem.* **2011**, *46*, 5435–5442. [[CrossRef](#)]
48. Fernandez-Bachiller, M.I.; Perez, C.; Monjas, L.; Rademann, J.; Rodriguez-Franco, M.I. New tacrine-4-oxo-4H-chromene hybrids as multifunctional agents for the treatment of Alzheimer's disease, with cholinergic, antioxidant, and beta-amyloid-reducing properties. *J. Med. Chem.* **2012**, *55*, 1303–1317. [[CrossRef](#)]
49. Makhaeva, G.F.; Rudakova, E.V.; Kovaleva, N.V.; Lushchekina, S.V.; Boltneva, N.P.; Proshin, A.N.; Shchegolkov, E.V.; Burgart, Y.V.; Saloutin, V.I. Cholinesterase and carboxylesterase inhibitors as pharmacological agents. *Russ. Chem. Bull.* **2019**, *68*, 967–984. [[CrossRef](#)]

50. Makhaeva, G.F.; Kovaleva, N.V.; Boltneva, N.P.; Lushchekina, S.V.; Rudakova, E.V.; Stupina, T.S.; Terentiev, A.A.; Serkov, I.V.; Proshin, A.N.; Radchenko, E.V.; et al. Conjugates of tacrine and 1,2,4-thiadiazole derivatives as new potential multifunctional agents for Alzheimer's disease treatment: Synthesis, quantum-chemical characterization, molecular docking, and biological evaluation. *Bioorg. Chem.* **2020**, *94*, 103387. [[CrossRef](#)]
51. Minarini, A.; Milelli, A.; Simoni, E.; Rosini, M.; Bolognesi, M.L.; Marchetti, C.; Tumiatti, V. Multifunctional tacrine derivatives in Alzheimer's disease. *Curr. Top. Med. Chem.* **2013**, *13*, 1771–1786. [[CrossRef](#)] [[PubMed](#)]
52. Girek, M.; Szymański, P. Tacrine hybrids as multi-target-directed ligands in Alzheimer's disease: Influence of chemical structures on biological activities. *Chem. Pap. Chem. Zvesti* **2018**, *73*, 269–289. [[CrossRef](#)]
53. Milelli, A.; De Simone, A.; Ticchi, N.; Chen, H.H.; Betari, N.; Andrisano, V.; Tumiatti, V. Tacrine-based multifunctional agents in Alzheimer's disease: An old story in continuous development section sign. *Curr. Med. Chem.* **2017**, *24*, 3522–3546. [[CrossRef](#)] [[PubMed](#)]
54. Spilovska, K.; Korabecny, J.; Nepovimova, E.; Dolezal, R.; Mezeiova, E.; Soukup, O.; Kuca, K. Multitarget tacrine hybrids with neuroprotective properties to confront Alzheimer's disease. *Curr. Top. Med. Chem.* **2017**, *17*, 1006–1026. [[CrossRef](#)] [[PubMed](#)]
55. Wu, W.Y.; Dai, Y.C.; Li, N.G.; Dong, Z.X.; Gu, T.; Shi, Z.H.; Xue, X.; Tang, Y.P.; Duan, J.A. Novel multitarget-directed tacrine derivatives as potential candidates for the treatment of Alzheimer's disease. *J. Enzym. Inhib. Med. Chem.* **2017**, *32*, 572–587. [[CrossRef](#)] [[PubMed](#)]
56. Przybyłowska, M.; Kowalski, S.; Dzierzbicka, K.; Inkielewicz-Stepniak, I. Therapeutic Potential of Multifunctional Tacrine Analogues. *Curr. Neuropharmacol.* **2019**, *17*, 472–490. [[CrossRef](#)]
57. AlFadly, E.D.; Elzahhar, P.A.; Tramarin, A.; Elkazaz, S.; Shaltout, H.; Abu-Serie, M.M.; Janockova, J.; Soukup, O.; Ghareeb, D.A.; El-Yazbi, A.F.; et al. Tackling neuroinflammation and cholinergic deficit in Alzheimer's disease: Multi-target inhibitors of cholinesterases, cyclooxygenase-2 and 15-lipoxygenase. *Eur. J. Med. Chem.* **2019**, *167*, 161–186. [[CrossRef](#)]
58. Supuran, C.T. Special Issue: Sulfonamides. *Molecules* **2017**, *22*, 1642. [[CrossRef](#)]
59. Apaydin, S.; Torok, M. Sulfonamide derivatives as multi-target agents for complex diseases. *Bioorg. Med. Chem. Lett.* **2019**, *29*, 2042–2050. [[CrossRef](#)]
60. Bonardi, A.; Nocentini, A.; Bua, S.; Combs, J.; Lomelino, C.; Andring, J.; Lucarini, L.; Sgambellone, S.; Masini, E.; McKenna, R.; et al. Sulfonamide Inhibitors of Human Carbonic Anhydrases Designed through a Three-Tails Approach: Improving Ligand/Isoform Matching and Selectivity of Action. *J. Med. Chem.* **2020**, *63*, 7422–7444. [[CrossRef](#)]
61. Nocentini, A.; Supuran, C.T. Advances in the structural annotation of human carbonic anhydrases and impact on future drug discovery. *Expert Opin. Drug Discov.* **2019**, *14*, 1175–1197. [[CrossRef](#)] [[PubMed](#)]
62. Supuran, C.T. Carbonic anhydrase inhibitors and their potential in a range of therapeutic areas. *Expert Opin. Ther. Pat.* **2018**, *28*, 709–712. [[CrossRef](#)] [[PubMed](#)]
63. Bag, S.; Tulsan, R.; Sood, A.; Cho, H.; Redjeb, H.; Zhou, W.; LeVine, H., III; Torok, B.; Torok, M. Sulfonamides as multifunctional agents for Alzheimer's disease. *Bioorg. Med. Chem. Lett.* **2015**, *25*, 626–630. [[CrossRef](#)]
64. Soyer, Z.; Uysal, S.; Parlar, S.; Tarikogullari Dogan, A.H.; Alptuzun, V. Synthesis and molecular docking studies of some 4-phthalimidobenzenesulfonamide derivatives as acetylcholinesterase and butyrylcholinesterase inhibitors. *J. Enzym. Inhib. Med. Chem.* **2017**, *32*, 13–19. [[CrossRef](#)] [[PubMed](#)]
65. Akocak, S.; Boga, M.; Lolak, N.; Tuneg, M.; Sanku, R.K.K. Design, synthesis and biological evaluation of 1,3-diaryltriazene-substituted sulfonamides as antioxidant, acetylcholinesterase and butyrylcholinesterase inhibitors. *J. Turk. Chem. Soc. Sect. Chem.* **2019**. [[CrossRef](#)]
66. Taslimi, P.; Sujayev, A.; Mamedova, S.; Kalin, P.; Gulcin, I.; Sadeghian, N.; Beydemir, S.; Kufrevioglu, O.I.; Alwasel, S.H.; Farzaliyev, V.; et al. Synthesis and bioactivity of several new hetaryl sulfonamides. *J. Enzym. Inhib. Med. Chem.* **2017**, *32*, 137–145. [[CrossRef](#)]
67. Kosak, U.; Knez, D.; Coquelle, N.; Brus, B.; Pislár, A.; Nachon, F.; Brazzolotto, X.; Kos, J.; Colletier, J.P.; Gobec, S. N-Propargylpiperidines with naphthalene-2-carboxamide or naphthalene-2-sulfonamide moieties: Potential multifunctional anti-Alzheimer's agents. *Bioorg. Med. Chem.* **2017**, *25*, 633–645. [[CrossRef](#)]
68. Gouda, M.A.; Hussein, B.H.M. Synthesis and Anti-Oxidant Evaluation of Some Novel Sulfa Drugs. *Lett. Drug Des. Discov.* **2017**, *14*, 1425–1432. [[CrossRef](#)]

69. Ulus, R.; Zengin Kurt, B.; Gazioglu, I.; Kaya, M. Microwave assisted synthesis of novel hybrid tacrine-sulfonamide derivatives and investigation of their antioxidant and anticholinesterase activities. *Bioorg. Chem.* **2017**, *70*, 245–255. [[CrossRef](#)]
70. Swetha, R.; Kumar, D.; Gupta, S.K.; Ganeshpurkar, A.; Singh, R.; Gutti, G.; Kumar, D.; Jana, S.; Krishnamurthy, S.; Singh, S.K. Multifunctional hybrid sulfonamides as novel therapeutic agents for Alzheimer's disease. *Future Med. Chem.* **2019**, *11*, 3161–3178. [[CrossRef](#)]
71. Makhaeva, G.F.; Kovaleva, N.V.; Lushchekina, S.V.; Rudakova, E.V.; Boltneva, N.P.; Proshin, A.N.; Lednev, B.V.; Serkov, I.V.; Bachurin, S.O. Conjugates of Tacrine and Its Cyclic Homologues with p-Toluenesulfonamide as Novel Acetylcholinesterase and Butyrylcholinesterase Inhibitors. *Dokl. Biochem. Biophys.* **2018**, *483*, 369–373. [[CrossRef](#)] [[PubMed](#)]
72. Tang, H.; Zhao, L.Z.; Zhao, H.T.; Huang, S.L.; Zhong, S.M.; Qin, J.K.; Chen, Z.F.; Huang, Z.S.; Liang, H. Hybrids of oxoisoaporphine-tacrine congeners: Novel acetylcholinesterase and acetylcholinesterase-induced beta-amyloid aggregation inhibitors. *Eur. J. Med. Chem.* **2011**, *46*, 4970–4979. [[CrossRef](#)] [[PubMed](#)]
73. Makhaeva, G.F.; Lushchekina, S.V.; Boltneva, N.P.; Sokolov, V.B.; Grigoriev, V.V.; Serebryakova, O.G.; Vikhareva, E.A.; Aksinenko, A.Y.; Barreto, G.E.; Aliev, G.; et al. Conjugates of g-carbolines and phenothiazine as new selective inhibitors of butyrylcholinesterase and blockers of NMDA receptors for Alzheimer disease. *Sci. Rep.* **2015**, *5*, 13164. [[CrossRef](#)] [[PubMed](#)]
74. Makhaeva, G.F.; Rudakova, E.V.; Serebryakova, O.G.; Aksinenko, A.Y.; Lushchekina, S.V.; Bachurin, S.O.; Richardson, R.J. Esterase profiles of organophosphorus compounds in vitro predict their behavior in vivo. *Chem. Biol. Interact.* **2016**, *259*, 332–342. [[CrossRef](#)] [[PubMed](#)]
75. Makhaeva, G.F.; Boltneva, N.P.; Lushchekina, S.V.; Serebryakova, O.G.; Stupina, T.S.; Terentiev, A.A.; Serkov, I.V.; Proshin, A.N.; Bachurin, S.O.; Richardson, R.J. Synthesis, molecular docking and biological evaluation of N,N-disubstituted 2-aminothiazolines as a new class of butyrylcholinesterase and carboxylesterase inhibitors. *Bioorg. Med. Chem.* **2016**, *24*, 1050–1062. [[CrossRef](#)]
76. Makhaeva, G.F.; Radchenko, E.V.; Palyulin, V.A.; Rudakova, E.V.; Aksinenko, A.Y.; Sokolov, V.B.; Zefirov, N.S.; Richardson, R.J. Organophosphorus compound esterase profiles as predictors of therapeutic and toxic effects. *Chem. Biol. Interact.* **2013**, *203*, 231–237. [[CrossRef](#)]
77. Makhaeva, G.F.; Radchenko, E.V.; Baskin, I.I.; Palyulin, V.A.; Richardson, R.J.; Zefirov, N.S. Combined QSAR studies of inhibitor properties of O-phosphorylated oximes toward serine esterases involved in neurotoxicity, drug metabolism and Alzheimer's disease. *SAR QSAR Environ. Res.* **2012**, *23*, 627–647. [[CrossRef](#)]
78. Pang, Y.P.; Quiram, P.; Jelacic, T.; Hong, F.; Brimijoin, S. Highly potent, selective, and low cost bis-tetrahydroaminacrine inhibitors of acetylcholinesterase. Steps toward novel drugs for treating Alzheimer's disease. *J. Biol. Chem.* **1996**, *271*, 23646–23649. [[CrossRef](#)]
79. Chen, Y.; Sun, J.; Peng, S.; Liao, H.; Zhang, Y.; Lehmann, J. Tacrine-flurbiprofen hybrids as multifunctional drug candidates for the treatment of Alzheimer's disease. *Arch. Pharm. (Weinh.)* **2013**, *346*, 865–871. [[CrossRef](#)]
80. Czarnecka, K.; Szymanski, P.; Girek, M.; Mikiciuk-Olasik, E.; Skibinski, R.; Kabzinski, J.; Majsterek, I.; Malawska, B.; Jonczyk, J.; Bajda, M. Tetrahydroacridine derivatives with fluorobenzoic acid moiety as multifunctional agents for Alzheimer's disease treatment. *Bioorg. Chem.* **2017**, *72*, 315–322. [[CrossRef](#)]
81. Korabecny, J.; Andrs, M.; Nepovimova, E.; Dolezal, R.; Babkova, K.; Horova, A.; Malinak, D.; Mezeiova, E.; Gorecki, L.; Sepsova, V.; et al. 7-Methoxytacrine-p-Anisidine Hybrids as Novel Dual Binding Site Acetylcholinesterase Inhibitors for Alzheimer's Disease Treatment. *Molecules* **2015**, *20*, 22084–22101. [[CrossRef](#)] [[PubMed](#)]
82. Spilovska, K.; Korabecny, J.; Horova, A.; Musilek, K.; Nepovimova, E.; Drtinova, L.; Gazova, Z.; Siposova, K.; Dolezal, R.; Jun, D.; et al. Design, synthesis and in vitro testing of 7-methoxytacrine-amantadine analogues: A novel cholinesterase inhibitors for the treatment of Alzheimer's disease. *Med. Chem. Res.* **2015**, *24*, 2645–2655. [[CrossRef](#)]
83. Makhaeva, G.F.; Shevtsova, E.F.; Boltneva, N.P.; Lushchekina, S.V.; Kovaleva, N.V.; Rudakova, E.V.; Bachurin, S.O.; Richardson, R.J. Overview of novel multifunctional agents based on conjugates of gamma-carbolines, carbazoles, tetrahydrocarbazoles, phenothiazines, and aminoadamantanes for treatment of Alzheimer's disease. *Chem. Biol. Interact.* **2019**, *308*, 224–234. [[CrossRef](#)] [[PubMed](#)]

84. Makhaeva, G.F.; Shevtsova, E.F.; Aksinenko, A.Y.; Kovaleva, N.V.; Boltneva, N.P.; Lushchekina, S.V.; Rudakova, E.V.; Pushkareva, E.A.; Serkova, T.P.; Dubova, L.G.; et al. Bis- γ -carbolines as new potential multitarget agents for Alzheimer's disease. *Pure Appl. Chem.* **2020**. [[CrossRef](#)]
85. Sussman, J.L.; Harel, M.; Frolow, F.; Oefner, C.; Goldman, A.; Toker, L.; Silman, I. Atomic structure of acetylcholinesterase from *Torpedo californica*: A prototypic acetylcholine-binding protein. *Science* **1991**, *253*, 872–879. [[CrossRef](#)]
86. Saxena, A.; Redman, A.M.; Jiang, X.; Lockridge, O.; Doctor, B.P. Differences in active site gorge dimensions of cholinesterases revealed by binding of inhibitors to human butyrylcholinesterase. *Biochemistry* **1997**, *36*, 14642–14651. [[CrossRef](#)]
87. Wlodek, S.T.; Clark, T.W.; Scott, L.R.; McCammon, J.A. Molecular Dynamics of Acetylcholinesterase Dimer Complexed with Tacrine. *J. Am. Chem. Soc.* **1997**, *119*, 9513–9522. [[CrossRef](#)]
88. Masson, P.; Lushchekina, S.V. Slow-binding inhibition of cholinesterases, pharmacological and toxicological relevance. *Arch. Biochem. Biophys.* **2016**, *593*, 60–68. [[CrossRef](#)]
89. Masson, P.; Froment, M.-T.; Fortier, P.-L.; Visicchio, J.-E.; Bartels, C.F.; Lockridge, O. Butyrylcholinesterase-catalysed hydrolysis of aspirin, a negatively charged ester, and aspirin-related neutral esters. *Biochim. Biophys. Acta Protein Struct. Mol. Enzymol.* **1998**, *1387*, 41–52. [[CrossRef](#)]
90. Kharlamova, A.D.; Lushchekina, S.V.; Petrov, K.A.; Kots, E.D.; Nachon, F.; Villard-Wandhammer, M.; Zueva, I.V.; Krejci, E.; Reznik, V.S.; Zobov, V.V.; et al. Slow-binding inhibition of acetylcholinesterase by an alkylammonium derivative of 6-methyluracil: Mechanism and possible advantages for myasthenia gravis treatment. *Biochem. J.* **2016**, *473*, 1225–1236. [[CrossRef](#)]
91. Sawatzky, E.; Wehle, S.; Kling, B.; Wendrich, J.; Bringmann, G.; Sottriffer, C.A.; Heilmann, J.; Decker, M. Discovery of Highly Selective and Nanomolar Carbamate-Based Butyrylcholinesterase Inhibitors by Rational Investigation into Their Inhibition Mode. *J. Med. Chem.* **2016**, *59*, 2067–2082. [[CrossRef](#)] [[PubMed](#)]
92. Lushchekina, S.V.; Makhaeva, G.F.; Novichkova, D.A.; Zueva, I.V.; Kovaleva, N.V.; Richardson, R.J. Supercomputer modeling of dual-site acetylcholinesterase (AChE) inhibition. *Supercomput. Front. Innov.* **2018**, *5*, 89–97. [[CrossRef](#)]
93. Taylor, P.; Lappi, S. Interaction of fluorescence probes with acetylcholinesterase. Site and specificity of propidium binding. *Biochemistry* **1975**, *14*, 1989–1997. [[CrossRef](#)] [[PubMed](#)]
94. Ellman, G.L.; Courtney, K.D.; Andres, V., Jr.; Feather-Stone, R.M. A new and rapid colorimetric determination of acetylcholinesterase activity. *Biochem. Pharmacol.* **1961**, *7*, 88–95. [[CrossRef](#)]
95. Sterri, S.H.; Johnsen, B.A.; Fonnum, F. A radiochemical assay method for carboxylesterase, and comparison of enzyme activity towards the substrates methyl [1-¹⁴C] butyrate and 4-nitrophenyl butyrate. *Biochem. Pharmacol.* **1985**, *34*, 2779–2785. [[CrossRef](#)]
96. Taylor, P.; Lwebuga-Mukasa, J.; Lappi, S.; Rademacher, J. Propidium—A fluorescence probe for a peripheral anionic site on acetylcholinesterase. *Mol. Pharmacol.* **1974**, *10*, 703–708.
97. Re, R.; Pellegrini, N.; Proteggente, A.; Pannala, A.; Yang, M.; Rice-Evans, C. Antioxidant activity applying an improved ABTS radical cation decolorization assay. *Free Radic. Biol. Med.* **1999**, *26*, 1231–1237. [[CrossRef](#)]
98. Cheung, J.; Rudolph, M.J.; Burshteyn, F.; Cassidy, M.S.; Gary, E.N.; Love, J.; Franklin, M.C.; Height, J.J. Structures of human acetylcholinesterase in complex with pharmacologically important ligands. *J. Med. Chem.* **2012**, *55*, 10282–10286. [[CrossRef](#)]
99. Nicolet, Y.; Lockridge, O.; Masson, P.; Fontecilla-Camps, J.C.; Nachon, F. Crystal structure of human butyrylcholinesterase and of its complexes with substrate and products. *J. Biol. Chem.* **2003**, *278*, 41141–41147. [[CrossRef](#)]
100. Masson, P.; Lushchekina, S.; Schopfer, L.M.; Lockridge, O. Effects of viscosity and osmotic stress on the reaction of human butyrylcholinesterase with cresyl saligenin phosphate, a toxicant related to aerotoxic syndrome: Kinetic and molecular dynamics studies. *Biochem. J.* **2013**, *454*, 387–399. [[CrossRef](#)]
101. Schmidt, M.W.; Baldridge, K.K.; Boatz, J.A.; Elbert, S.T.; Gordon, M.S.; Jensen, J.H.; Koseki, S.; Matsunaga, N.; Nguyen, K.A.; Su, S.; et al. General atomic and molecular electronic structure system. *J. Comput. Chem.* **1993**, *14*, 1347–1363. [[CrossRef](#)]
102. Löwdin, P.-O. On the nonorthogonality problem. In *Advances in Quantum Chemistry*; Per-Olov, L., Ed.; Academic Press: New York, NY, USA, 1970; Volume 5, pp. 185–199.

103. Morris, G.M.; Huey, R.; Lindstrom, W.; Sanner, M.F.; Belew, R.K.; Goodsell, D.S.; Olson, A.J. AutoDock4 and AutoDockTools4: Automated docking with selective receptor flexibility. *J. Comput. Chem.* **2009**, *30*, 2785–2791. [[CrossRef](#)]
104. Morris, G.M.; Goodsell, D.S.; Halliday, R.S.; Huey, R.; Hart, W.E.; Belew, R.K.; Olson, A.J. Automated docking using a Lamarckian genetic algorithm and an empirical binding free energy function. *J. Comput. Chem.* **1998**, *19*, 1639–1662. [[CrossRef](#)]
105. Radchenko, E.V.; Dyabina, A.S.; Palyulin, V.A.; Zefirov, N.S. Prediction of human intestinal absorption of drug compounds. *Russ. Chem. Bull.* **2016**, *65*, 576–580. [[CrossRef](#)]
106. Dyabina, A.S.; Radchenko, E.V.; Palyulin, V.A.; Zefirov, N.S. Prediction of blood-brain barrier permeability of organic compounds. *Dokl. Biochem. Biophys.* **2016**, *470*, 371–374. [[CrossRef](#)] [[PubMed](#)]
107. Radchenko, E.V.; Rulev, Y.A.; Safanyaev, A.Y.; Palyulin, V.A.; Zefirov, N.S. Computer-aided estimation of the hERG-mediated cardiotoxicity risk of potential drug components. *Dokl. Biochem. Biophys.* **2017**, *473*, 128–131. [[CrossRef](#)] [[PubMed](#)]
108. ADMET Prediction Service. Available online: <http://qsar.chem.msu.ru/admet/> (accessed on 1 April 2020).
109. Sushko, I.; Novotarskyi, S.; Korner, R.; Pandey, A.K.; Rupp, M.; Teetz, W.; Brandmaier, S.; Abdelaziz, A.; Prokopenko, V.V.; Tanchuk, V.Y.; et al. Online chemical modeling environment (OCHEM): Web platform for data storage, model development and publishing of chemical information. *J. Comput. Aided. Mol. Des.* **2011**, *25*, 533–554. [[CrossRef](#)]
110. Bickerton, G.R.; Paolini, G.V.; Besnard, J.; Muresan, S.; Hopkins, A.L. Quantifying the chemical beauty of drugs. *Nat. Chem.* **2012**, *4*, 90–98. [[CrossRef](#)]
111. RDKit: Open-Source Cheminformatics Software. Available online: <http://www.rdkit.org> (accessed on 1 December 2019).
112. Voevodin, V.; Antonov, A.; Nikitenko, D.; Shvets, P.; Sobolev, S.; Sidorov, I.; Stefanov, K.; Voevodin, V.; Zhumatiy, S. Supercomputer Lomonosov-2: Large scale, deep monitoring and fine analytics for the user community. *Supercomput. Front. Innov.* **2019**, *6*, 4–11. [[CrossRef](#)]

Sample Availability: Samples of the compounds are not available.



© 2020 by the authors. Licensee MDPI, Basel, Switzerland. This article is an open access article distributed under the terms and conditions of the Creative Commons Attribution (CC BY) license (<http://creativecommons.org/licenses/by/4.0/>).